

Multi-Reference Entropy Model for Learned Image Compression

Wei Jiang¹, Jiayu Yang¹, Yongqi Zhai¹, Ronggang Wang^{1,2}

¹ Shenzhen Graduate School, Peking University, Shenzhen, China

² Peng Cheng Laboratory, Shenzhen, China

wei.jiang1999@outlook.com

Abstract

Recently, learned image compression has achieved remarkable performance. Entropy model, which accurately estimates the distribution of latent representation, plays an important role in boosting rate distortion performance. Most entropy models capture correlations in one dimension. However, there are channel-wise, local and global spatial correlations in latent representation. To address this issue, we propose multi-reference entropy models MEM and MEM⁺ to capture channel, local and global spatial contexts. We divide latent representation into slices. When decoding current slice, we use previously decoded slices as contexts and use attention map of previously decoded slice to predict global correlations in current slice. To capture local contexts, we propose enhanced checkerboard context capturing to avoid performance degradation while retaining two-pass decoding. Based on MEM and MEM⁺, we propose image compression models MLIC and MLIC⁺. Extensive experimental evaluations have shown that our MLIC and MLIC⁺ achieve state-of-the-art performance and they reduce BD-rate by 9.77% and 13.09% on Kodak dataset over VVC when measured in PSNR.

Introduction

Due to the rise of social media, with tens of millions of images being generated and transmitted on the web every second, it is important for service providers to find more efficient and effective image compression methods to save bandwidth. Although traditional coding methods like JPEG (Pennebaker and Mitchell 1992), JPEG2000 (Charrier, Cruz, and Larsson 1999), BPG (Bellard 2015), VVC (JVET 2021) have achieved good performance, they rely on manual design for each module which is independent from each other, making joint optimization impossible.

Recently, various learned image compression models (Toderici et al. 2016; Ballé, Laparra, and Simoncelli 2017; Rippel and Bourdev 2017; Toderici et al. 2017; Theis et al. 2017; Johnston et al. 2018; Mentzer et al. 2018; Li et al. 2018; Lee, Cho, and Beack 2019; Ayzik and Avidan 2020; Hu, Yang, and Liu 2020; Lin et al. 2020; Li et al. 2020; Akbari et al. 2021; Guo et al. 2021b; Ma et al. 2020; Zhu et al. 2022; Koyuncu, Gao, and Steinbach 2022) have been proposed, and they have achieved remarkable performance. Some learned image compression models (Cheng et al. 2020; Chen et al. 2021; Minnen and Singh 2020; Wu et al. 2021; Xie, Cheng, and Chen 2021; Lu et al. 2022) are

already comparable to advanced traditional method VVC. Most of these models are based on variational autoencoders (Kingma and Welling 2014), following the transform, quantization, entropy coding, and inverse transform process. Transform and entropy coding play an important role in boosting model performance. The transform process turns an input image into a compact latent representation which is easier to be compressed. An entropy model is used to estimate the entropy of latent representation. A powerful and accurate entropy model usually leads to fewer bits.

The state-of-the-art learned image compression models (Gao et al. 2021; Chen, Xu, and Wang 2022; He et al. 2022) usually equip entropy model with a hyperior model (Ballé et al. 2018) or a context model (Minnen, Ballé, and Toderici 2018) to estimate conditional entropy and use conditional probabilities for coding. Context models usually model probabilities and correlations in different dimensions, which can be divided into three kinds: local spatial context model, global spatial context model and channel context model (Minnen and Singh 2020). Most of the methods model conditional probabilities in a single dimension. However, we find there are correlations in all dimensions. Modeling probabilities and correlations in a single dimension leads to inaccurate conditional probabilities and hinder the performance, which inspires us to design multi-reference entropy models MEM and MEM⁺. In our MEM and MEM⁺, we capture local spatial, global spatial and channel contexts. Based on MEM and MEM⁺, we propose MLIC and MLIC⁺, which achieve state-of-art performance. To capture correlations between channels, we divide the latent representations into several slices. When compressing a slice, the previous compressed slices are used as its contexts and a channel fusion module is used to get the channel information from previous slices. We conduct local and global context modeling for every slice separately. An auto-regressive local context model leads to serial decoding, while a checkerboard context model (He et al. 2021) can achieve two pass parallel decoding which divides latent representations into anchor and non-anchor part. Compared to auto-regressive context model, checkerboard context model leads to up to 4% performance degradation. We propose two different ways to address it, stacked checkerboard context modeling and overlapped checkerboard window attention. Some previous methods focused on global context modeling (Qian et al.

2021; Guo et al. 2021a) cooperate with serial local spatial context model, which will cause slower decoding. Assuming the similar spatial correlations in different slices, for the i -th slice, we first compute the attention map of decoded $i - 1$ -th slice, which is used to predict the global correlations in i -th slice. We also explore the global correlations in adjacent slices. Our approach for global spatial context modeling can work well with checkerboard-like patterns by attention masks. Finally, we fuse channel, local, global contexts and side information to compute the distribution of latent representations. Our contributions are summarized as follows:

- We design multi-reference entropy models MEM and MEM⁺ which combine local spatial, global spatial and channel contexts and hyper-prior side information. Based on MEM and MEM⁺, we propose MLIC and MLIC⁺, which achieve state-of-the-art performance. We successfully explore the potential of an entropy model.
- To capture local spatial contexts, we design stacked checkerboard context module and checkerboard attention to address the degradation of checkerboard context modeling while retaining two-pass decoding.
- We divide latent representation into slices and use the attention map of previous decoded slice to predict the global correlations in current slice. We also explore global correlations between adjacent slices.

Related Works

Learned Lossy Image Compression

According to rate-distortion optimization, more bits lead to lower distortion. It is a trade-off. Lagrange multiplier λ is used to adjust the weight of distortion to control target bit-rate. The optimization target is

$$\mathcal{L} = \mathcal{R} + \lambda \mathcal{D}, \quad (1)$$

\mathcal{D} means distortion, \mathcal{R} means bit-rate.

The basic learned image compression framework (Ballé, Laparra, and Simoncelli 2017) consists analysis transform g_a , quantization Q , synthesis transform g_s and an entropy model to estimate rates. The process can be formulated as:

$$\mathbf{y} = g_a(\mathbf{x}; \theta), \hat{\mathbf{y}} = Q(\mathbf{y}), \hat{\mathbf{x}} = g_s(\hat{\mathbf{y}}; \phi), \quad (2)$$

where \mathbf{x} is the input image, g_a transform the \mathbf{x} to compact latent representation \mathbf{y} . \mathbf{y} is quantized to $\hat{\mathbf{y}}$ for entropy coding. $\hat{\mathbf{x}}$ is the decompressed image. θ and ϕ are parameters of g_a and g_s . Quantization leads to non-differentiability, which can be addressed by adding uniform noise $\mathcal{U}(-0.5, 0.5)$ (Ballé, Laparra, and Simoncelli 2017) or assuming the gradient as 1 (Theis et al. 2017) during training. GDN/IGDN (Ballé, Laparra, and Simoncelli 2016) layers are used to improve non-linearity. In the basic model, the probability model is a factorized or a non-adaptive density model because there is no information shared by encoder and decoder. The estimated rate of $\hat{\mathbf{y}}$ is $\mathbb{E}[-\log_2 p_{\hat{\mathbf{y}}}(\hat{\mathbf{y}})]$.

A hyper-prior model is first introduced in (Ballé et al. 2018), which extracts side information $\hat{\mathbf{z}}$ from \mathbf{y} . Hyper-prior model estimate distribution of $\hat{\mathbf{y}}$ from $\hat{\mathbf{z}}$. The rate of $\hat{\mathbf{y}}$ is $\mathbb{E}[-\log_2 p_{\hat{\mathbf{y}}|\hat{\mathbf{z}}}(\hat{\mathbf{y}}|\hat{\mathbf{z}})]$ and a uni-variate Gaussian distribution model for the hyper-prior is used. Some works extend

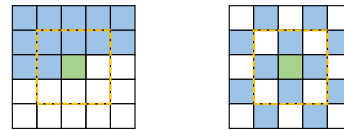


Figure 1: Autoregressive context model $g_{lc,ar}$ (left) and checkerboard context model $g_{lc,ckbd}$ (right). Blue squares are decoded symbols which are contexts, green square is the symbol to be decoded and white squares are symbols that are not decoded. Orange dotted box is the receptive field.

it to a mean and scale Gaussian distribution (Minnen, Ballé, and Toderici 2018), asymmetric Gaussian distribution (Cui et al. 2021) and Gaussian mixture model (Cheng et al. 2020; Liu et al. 2020) for more flexible distribution modeling.

Context-conditional Entropy Model

Context-conditional models are based on the principle that the conditional entropy is less than or equal to the entropy. Many works (Minnen, Ballé, and Toderici 2018; Minnen and Singh 2020) have been proposed for more accurate context modeling, including local spatial context models, global spatial context models and channel-wise context models.

Local spatial context models capture correlations between adjacent symbols. In (Minnen, Ballé, and Toderici 2018), a masked convolutional layer is used to capture local correlations between $\hat{\mathbf{y}}_i$ and symbols $\hat{\mathbf{y}}_{<i}$. In (Zhou et al. 2019), three parallel convolutional layers with different kernel size are used to capture correlations. Such kind of context models forward correlations, which leads to serial decoding. He et al. (He et al. 2021) divide latent representation $\hat{\mathbf{y}}$ into two parts $\hat{\mathbf{y}}_a$ and $\hat{\mathbf{y}}_{na}$ and use a checkerboard convolution to extract contexts of $\hat{\mathbf{y}}_{na}$ from $\hat{\mathbf{y}}_a$, achieving two-pass parallel decoding. These context models are illustrated in Figure 1.

Some work aims to model correlations between distant symbols. In (Qian et al. 2021), neighbouring left and top symbols are used as basis to compute the cosine similarity between the target symbols and its previous symbols. In (Guo et al. 2021a), latent representation are divided to 2 parts, the L_2 distances of symbols in the first slice are used to predict distant correlations in the second slice. In (Kim, Heo, and Lee 2022), the side information is divided to global side information and local side information which leads to extra bit-rates. Another problem is that these global context models are incorporated with serial autoregressive context model, which further increases decoding latency.

Minnen et al. (Minnen and Singh 2020) model contexts between channels. $\hat{\mathbf{y}}$ is evenly divided to slices, current slice $\hat{\mathbf{y}}^i$ is conditioned on previous decoded slices $\hat{\mathbf{y}}^{<i}$. According to the uneven distribution of information of every slice caused by channel-wise context model, an unevenly grouped channel-wise context model is proposed in (He et al. 2022).

Some local and channel-wise context models (Ma et al. 2021; He et al. 2022) have been proposed and achieve remarkable performance. However, the combination of local, global and channel context is not explored. The distant correlations in latent representation are general. If we model these correlations, we will receive a performance gain.

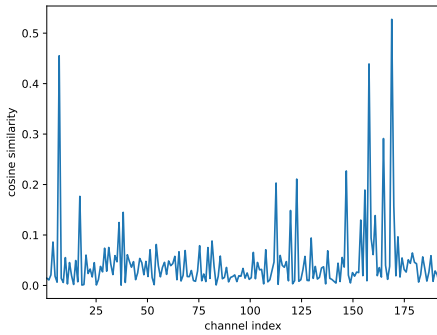


Figure 2: Absolute value of cosine similarity between the first channel and other channels of latent representation of Kodim19 extracted by Cheng’20 (Cheng et al. 2020)(optimized for MSE).

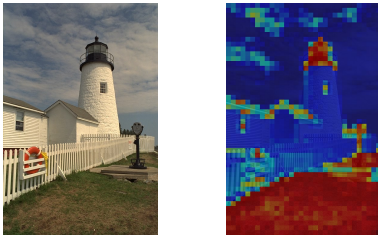


Figure 3: Heatmap of spatial cosine similarity of latent representation of Kodim19 extracted by Cheng’20 (Cheng et al. 2020) (optimized for MSE).

Method

Motivation

According to information theory, conditional entropy is less than or equal to the entropy.

$$\mathbb{E}[-\log_2 p_{\hat{\mathbf{y}}}(\hat{\mathbf{y}})] \geq \mathbb{E}[-\log_2 p_{\hat{\mathbf{y}}|\mathbf{ctx}}(\hat{\mathbf{y}}|\mathbf{ctx})], \quad (3)$$

where \mathbf{ctx} is the context of $\hat{\mathbf{y}}$. As long as there are correlations in latents $\hat{\mathbf{y}}$, the correlations can be used to save bits.

In Figure 2 and Figure 3, we first illustrate channel-wise correlations and spatial correlations in latent representation of Kodim19 extracted by Cheng’20 (Cheng et al. 2020). We use cosine similarity to measure correlations. In Figure 2, the similarity between some distant channels is at most more than 0.5 and the similarity of a few channels is larger than 0.1. Such correlations are hard for a spatial context model to capture, because spatial context model adopts the same mask for all channels when extracting contexts, which means there are always some correlations that cannot be captured. In Figure 3, symbols with the same color are of high correlations. In the bottom of Kodim19, the feature of grass is similar. However, a local context model is impossible to capture the correlation between the symbols in bottom-left corner and symbols in bottom-right corner because of the limited receptive field. The latent representation is with redundancy, which means there is potential to save bits by modeling such correlations. However, previous entropy models cannot model such correlations both in spatial and channel domain.

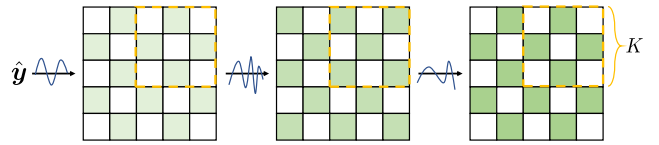


Figure 4: Stacked Checkerboard Context Module $g_{lc,stk}$. The figure illustrate changes of context information after every nonlinear transform. Green squares are context information.

	$g_{lc,stk}$	$g_{lc,attn}$	g_{ch}	$g_{gc,intra}$	$g_{gc,inter}$
MEM	✓		✓	✓	
MEM ⁺		✓	✓	✓	✓

Table 1: Settings of MEM and MEM⁺.

For a spatial context model, the interactions between channels are limited and for a channel-wise context model, there is no interaction in the current slice, which inspires us to design multi-reference entropy models. Our multi-reference entropy model capture correlations in the spatial and channel domain, which are introduced in following sections.

Multi-reference Entropy Model

We first give an overview of our proposed multi-reference entropy models MEM and MEM⁺ for channel, local and global spatial context capturing. Our MEM and MEM⁺ contains three parts: channel fusion module g_{ch} , local context module g_{lc} and global context module g_{gc} . We propose two different approaches: Stacked Checkerboard Context Module $g_{lc,stk}$ and Shifted Window-based Checkerboard Attention $g_{lc,attn}$ to capture local contexts. We divide global contexts into intra-slice and inter-slice contexts. We propose Intra-Slice Global Context Module $g_{gc,intra}$ and Inter-Slice Global Context Module $g_{gc,inter}$ to capture such correlations. We introduce these modules in the following sections. The structures of MEM and MEM⁺ are shown in Table 1.

Channel Fusion Module

To extract channel context, we first evenly divide latent representation $\hat{\mathbf{y}}$ into several slices $\{\hat{\mathbf{y}}^0, \hat{\mathbf{y}}^1, \dots, \hat{\mathbf{y}}^L\}$, L is the number of slices. Slice $\hat{\mathbf{y}}^i$ is conditioned on slices $\hat{\mathbf{y}}^{<i}$. We use a channel fusion module g_{ch} to squeeze and extract context information from $\hat{\mathbf{y}}^{<i}$ when encoding or decoding $\hat{\mathbf{y}}^i$. g_{ch} consists of three 3×3 convolutional layers. The channel context becomes $\Phi_{ch}^i = g_{ch}(\hat{\mathbf{y}}^{<i})$. The channel fusion module g_{ch} helps select the most relative channels and extract information beneficial for accurate probability estimation. Differnet from Minnen et al (Minnen and Singh 2020), we do not limit the number of slices that can be used as contexts to explore the potential of an entropy model. The channel number of each slic S is a hyper-parameter. Since there is no channel context for the 1-st slice, when decreasing S , the size of the 1-st slice becomes smaller, leading to more symbols in latent with channel contexts and slower decoding due to serial processing among slices. It’s a trade-off.

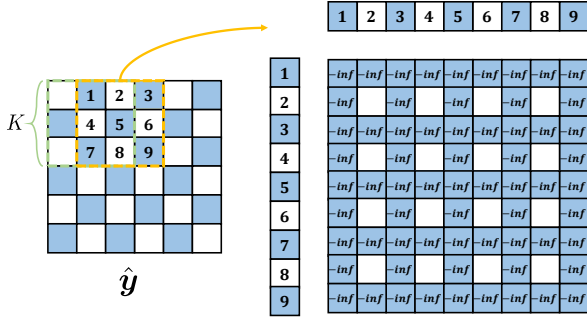


Figure 5: Mask of Shifted Window based Checkerboard Attention $g_{lc,attn}$. Blue squares are non-anchor part \hat{y}_{na} , white squares are anchor part \hat{y}_a . Green square and yellow square are two windows.

Following Minnen et al (Minnen and Singh 2020), we set S to 32 in our models.

Enhanced Checkerboard Context Capturing

The auto-regressive context model $g_{lc,ar}$ (Minnen, Ballé, and Toderici 2018) leads serial decoding, while checkerboard context model (He et al. 2021) makes parallel decoding possible. Our local context model is based on checkerboard context model. In checkerboard context model, only half of the symbols are conditioned on decoded symbols, which lead to a slight degradation. We propose two different ways to solve it from different perspectives. An example of auto-regressive and checkerboard context is illustrated in Figure 1.

Stacked Checkerboard Context Module The success of resnet (He et al. 2016) illustrates that increasing depth tends to improve expressiveness. In previous work (Minnen, Ballé, and Toderici 2018; Li et al. 2020; Cheng et al. 2020; He et al. 2021), local context model is a convolutional layer. In this model, we stack J convolutional layers in our model $g_{lc,stk}$, which brings non-linearity. According to the characteristics of checkerboard pattern, J should be an odd number. The odd-numbered convolution transfers the information extracted from the anchor part to the non-anchor part and the even-numbered convolution transfers the information extracted from the non-anchor part to the anchor part. The transfer process of context information is shown in the Figure 4 when J is 3. We set $J = 3$ to balance model performance and parameters and set kernel size $K = 5$.

Shifted-Window-based Checkerboard Attention Transformers (Vaswani et al. 2017) have been widely used in many vision tasks. It seems that transformers are more capable of modeling correlations than CNNs. The successes of swin-transformer (Liu et al. 2021) or window attention in compression (Lu et al. 2022; Zhu, Yang, and Cohen 2022; Zou, Song, and Zhang 2022) inspire us to design a window-based checkerboard attention $g_{lc,attn}$ for local context modeling. The latent representation \hat{y} is divided into $H \times W$ overlapped windows and the window size is $K \times K$. To ex-

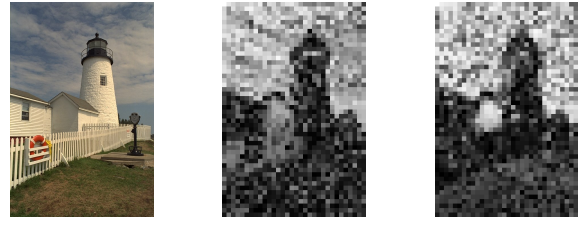


Figure 6: Cosine similarity in the spatial domain of different slices of latent representation of Kodim19 extracted by Cheng²⁰ (Cheng et al. 2020) (optimized for MSE).

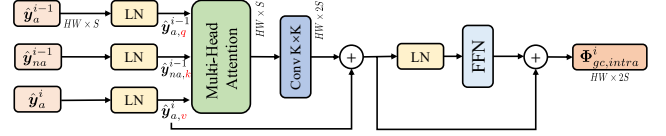


Figure 7: Intra-Slice Global Context Model $g_{gc,intra}$. S is the channel number of a slice.

tract local correlations, we first compute the attention map of each window. Same as convolutional checkerboard context model, interactions with non-anchor parts and in non-anchor parts are not allowed. An example of attention mask is illustrated in Figure 5. Such attention do not change the resolution of each window. We use a $K \times K$ convolutional layer to fusion local context information and make the size of local context same with that of latent representation before feeding it to a FFN. The process be formulated as:

$$\hat{y}_{attn}^i = \text{softmax} \left(\frac{\hat{y}_{a,q}^i \times (\hat{y}_{a,k}^i)^\top}{\sqrt{S}} + \text{mask} \right) \times \hat{y}_{a,v}^i, \quad (4)$$

$$\hat{y}_{conv}^i = \text{conv}_{K \times K}(\hat{y}_{attn}^i), \quad (5)$$

$$\Phi_{lc,attn}^i = \text{FFN}(\hat{y}_{conv}^i) + \hat{y}_{conv}^i, \quad (6)$$

where $\hat{y}_{a,q}^i, \hat{y}_{a,k}^i, \hat{y}_{a,v}^i = \text{Embed}(\hat{y}_a^i)$, \hat{y}_a^i is anchor part of i -th slice, mask the attention mask, S is the channel number of each slice.

The cost of such shifted-window based checkerboard attention $g_{lc,attn}$ is $\Omega(2K^4HWM + 4HWM^2)$, where M is the channel number of latent representation \hat{y} . When the slice number is L , the cost is $\Omega(2K^4HWM + 4HWM \frac{M^2}{L})$, which is linear with resolution of latent representation \hat{y} .

Global Spatial Context Capturing

We explore global correlations between non-anchor part \hat{y}_{na}^i and anchor part \hat{y}_a^i in a slice \hat{y}^i and between non-anchor part \hat{y}_{na}^i and slice \hat{y}^{i-1} by attention mechanisms.

Intra-Slice Global Context Module Due to codec consistency, it is impossible to know the global correlations between current symbols and other symbols during decoding. One solution is writing global correlations into code-stream, which causes extra bits. We notice the the similarity of global correlations between slices. When decoding current slice \hat{y}^i , decoded slice \hat{y}_{i-1} is helpful for estimating the

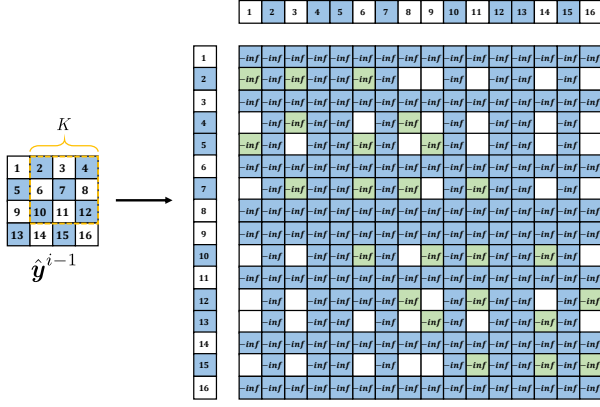


Figure 8: Mask of Intra-Slice Global Context Model $g_{gc,intra}$. Blue squares are non-anchor part $\hat{\mathbf{y}}_{na}^{i-1}$ and white squares are anchor part $\hat{\mathbf{y}}_a^{i-1}$ of slice $\hat{\mathbf{y}}^{i-1}$. The green squares are masked to avoid interactions in local receptive field. The orange dotted box is the receptive field of the local context model.

global correlations in slice $\hat{\mathbf{y}}^i$. We illustrate cosine similarity of two slices of Cheng’20 (Cheng et al. 2020) in Figure 6. Global correlations are similar despite differences in magnitude. Compared with CNN, transformers can capture much distant correlations. We use transformers to model global correlations. When compressing or decompressing $\hat{\mathbf{y}}^i$, we first compute the correlations between anchor part $\hat{\mathbf{y}}_a^{i-1}$ and non-anchor part $\hat{\mathbf{y}}_{na}^{i-1}$ of slice $\hat{\mathbf{y}}^{i-1}$, because the checkerboard local context model makes anchor visible when decoding non-anchor part. We multiply anchor part of current slice $\hat{\mathbf{y}}_a^i$ with attention map and feed it to a $K \times K$ convolutional layer because the prior that adjacent symbols have similar global correlations. The process of this Intra-Slice Global Context $g_{gc,inter}$ can be formulated as:

$$\hat{\mathbf{y}}_{attn}^i = \text{softmax} \left(\frac{\hat{\mathbf{y}}_{na,q}^{i-1} \times (\hat{\mathbf{y}}_{a,k}^{i-1})^\top}{\sqrt{S}} + \text{mask} \right) \times \hat{\mathbf{y}}_{a,v}^i, \quad (7)$$

$$\hat{\mathbf{y}}_{conv}^i = \text{conv}_{K \times K}(\hat{\mathbf{y}}_{attn}^i) + \hat{\mathbf{y}}_{a,v}^i, \quad (8)$$

$$\Phi_{gc,intra}^i = \text{FFN}(\hat{\mathbf{y}}_{conv}^i) + \hat{\mathbf{y}}_{conv}^i, \quad (9)$$

where $\hat{\mathbf{y}}_{na,q}^{i-1}, \hat{\mathbf{y}}_{a,k}^{i-1} = \text{Embed}(\hat{\mathbf{y}}^{i-1})$, $\hat{\mathbf{y}}_{a,v}^i = \text{Embed}(\hat{\mathbf{y}}_a^i)$. Note that interactions within $\hat{\mathbf{y}}_{na}^{i-1}$ and $\hat{\mathbf{y}}_a^{i-1}$ are masked. Local receptive fields are also masked to avoid degrading to local context model. *mask* is illustrated in Figure 8.

Inter-Slice Global Context Module Because of the global correlations between slices, we extend intra-slice global context to inter-slice global context. We explore the correlations between $\hat{\mathbf{y}}_{na}^i$ and $\hat{\mathbf{y}}^{i-1}$ by using $\hat{\mathbf{y}}_a^i$ as an approximation of $\hat{\mathbf{y}}_{na}^i$. The process of this Inter-Slice Global

	N	M	S	K	MEM	MEM^+
MLIC	192	192	32	5	✓	
MLIC ⁺	192	320	32	5		✓

Table 2: Settings of MLIC and MLIC⁺.

Context Model $g_{gc,inter}$ can be formulated as:

$$\hat{\mathbf{y}}_{attn}^i = \text{softmax} \left(\frac{\hat{\mathbf{y}}_q^{i-1} \times (\hat{\mathbf{y}}_{a,k}^i)^\top}{\sqrt{S}} + \text{mask} \right) \times \hat{\mathbf{y}}_v^{i-1}, \quad (10)$$

$$\hat{\mathbf{y}}_{conv}^i = \text{conv}_{K \times K}(\hat{\mathbf{y}}_{attn}^i) + \hat{\mathbf{y}}_v^{i-1}, \quad (11)$$

$$\Phi_{gc,inter}^i = \text{FFN}(\hat{\mathbf{y}}_{conv}^i) + \hat{\mathbf{y}}_{conv}^i, \quad (12)$$

where $\hat{\mathbf{y}}_q^{i-1}, \hat{\mathbf{y}}_v^{i-1} = \text{Embed}(\hat{\mathbf{y}}^{i-1})$, $\hat{\mathbf{y}}_{a,k}^i = \text{Embed}(\hat{\mathbf{y}}_a^i)$.

MLIC and MLIC⁺

We propose two models MLIC and MLIC⁺, which are illustrated in Figure 9. MLIC and MLIC⁺ share the same analysis, synthesis transform, hyper analysis and hyper synthesis, which are borrowed from Cheng’20 (Cheng et al. 2020), but we remove attention modules to reduce parameters. The hyper-parameters and settings of MLIC and MLIC⁺ is shown in Table 2. Same with Minnen et al. (Minnen and Singh 2020), we adopt STE round (Theis et al. 2017), Gaussian mean-scale entropy model and Latent Residual Prediction modules (Minnen and Singh 2020), which predicts quantization error based on hyper-prior and decoded slices. We illustrate the decompressing process of MLIC and MLIC⁺ in Figure 10. We use Equation 1 as our loss function and the estimated rate can be formulated as: $\mathcal{R} = \sum_{i=0}^L \mathcal{R}_a^i + \mathcal{R}_{na}^i$, where

$$\mathcal{R}_a^i = \mathbb{E}[-\log_2 p_{\hat{\mathbf{y}}_a^i | \Phi_{ch}^i, \Phi_h^i}(\hat{\mathbf{y}}_a^i | \Phi_{ch}^i, \Phi_h^i)], \quad (13)$$

$$\mathcal{R}_{na}^i = \mathbb{E}[-\log_2 p_{\hat{\mathbf{y}}_{na}^i | \Phi_{ch}^i, \Phi_h^i, \Phi_{lc}^i, \Phi_{gc}^i}(\hat{\mathbf{y}}_{na}^i | \Phi_{ch}^i, \Phi_h^i, \Phi_{lc}^i, \Phi_{gc}^i)]. \quad (14)$$

Experiments

Settings

We select 2×10^5 images from COCO2017 (Lin et al. 2014), DIV2K (Agustsson and Timofte 2017), ImageNet (Russakovsky et al. 2015) with resolution larger than 480×480 as our training set. We train our model on a single Tesla V100 GPU with various configurations of the Lagrange multiplier λ for different quality presets. We use MSE and MS-SSIM as distortion metrics. Following the settings of CompressAI (Bégaint et al. 2020), we set $\lambda \in \{18, 35, 67, 130, 250, 483\} \times 10^{-4}$ for MSE and $\lambda \in \{2.40, 4.58, 8.73, 16.64, 31.73, 60.50\}$ for MS-SSIM (Wang, Simoncelli, and Bovik 2003). We train each model with an Adam optimizer with $\beta_1 = 0.9, \beta_2 = 0.999$ and batch size is 8. We train each model for 2M steps. The learning rate starts at 10^{-4} and drops to 3×10^{-5} at 1.5M steps, drops to 10^{-5} at 1.8M steps, drops to 3×10^{-6} at 1.9M steps,

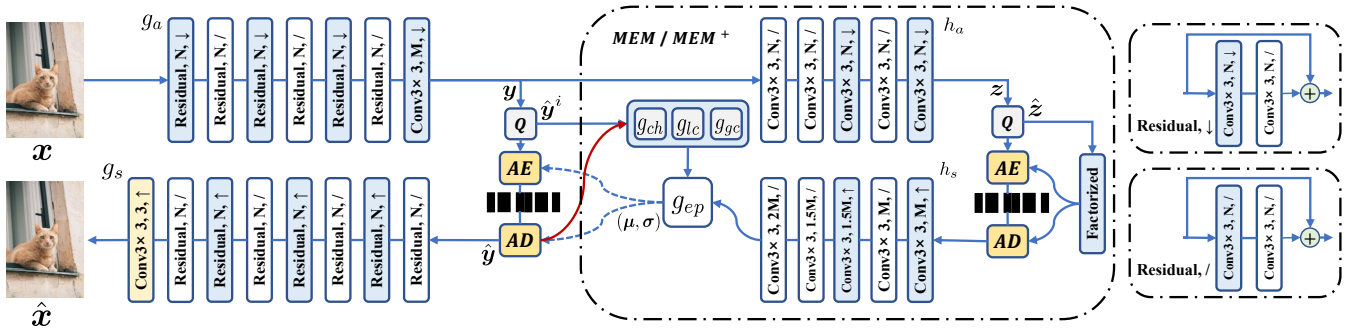


Figure 9: Overall architecture of MLIC and MLIC⁺. MLIC and MLIC⁺ is based on Cheng’20 (Cheng et al. 2020), but attention modules are removed and GMM is replaced with gaussian mean-scale model. M and N is the channel number of latent representation \hat{y} and side information \hat{z} respectively. \downarrow means down-sampling. $/$ means stride equals to 1.

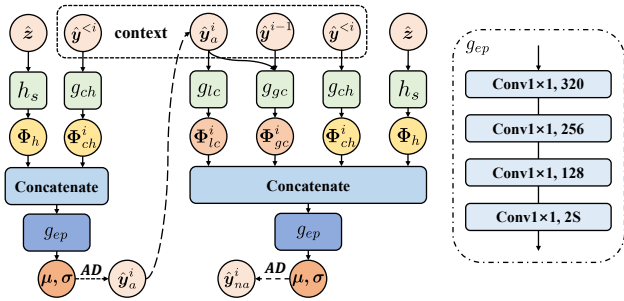


Figure 10: Multi-Reference Entropy Model MEM and MEM⁺. The figure illustrates the process of decoding a slice \hat{y}^i . S is the channel number of a slice.

Methods	Latency (s)				FLOPs (G)	
	Encoder		Decoder		Forward	
	Abs	Rel	Abs	Rel	Abs	Rel
Cheng’20 w/ checkerboard	0.21	1.00×	0.23	1.00×	406.76	1.00×
Cheng’20 w/o attention	3.11	14.81×	7.03	30.57×	376.15	0.92×
Cheng’20	3.41	16.24×	7.15	31.09×	415.62	1.02×
Xie’21	3.66	17.43×	7.63	36.33×	412.50	1.01×
MLIC(ours)	0.34	1.62×	0.25	1.09×	407.15	1.00×
MLIC ⁺ (ours)	0.42	2.00×	0.44	1.91×	500.78	1.23×

Table 3: Computational complexity of our and other methods. We evaluate complexity of encoding, decoding latency and forward Flops on Kodak dataset on a single Titan X. We use fvcore (Metaresearch 2019) library to evaluate Flops.

drops to 10^{-6} at 1.95M steps. During training, we random crop images to 256×256 patches during the first 1.2M steps, and crop images to 448×448 patches during the rest steps due to the sparsity of intra and inter slice attention mask shown in Figure 8. Large patches are beneficial for models to learn global references.

Performance

We evaluate our models on rate-distortion performance and codec efficiency.

Rate-Distortion Performance Figure 11 shows the rate-distortion performance on Kodak (Kodak 1993), CLIC Professional Valid (Toderici et al. 2020) and Tecnick (Asuni and Giachetti 2014) dataset. In Figure 11, we compare our MLIC and MLIC⁺ with classic and recent models (Minnen, Ballé, and Toderici 2018; Cheng et al. 2020; Minnen and Singh 2020; Xie, Cheng, and Chen 2021; Zou, Song, and Zhang 2022; He et al. 2022). Our MLIC and MLIC⁺ achieve state-of-the-art performance and they reduce BD-rate by 9.77% and 13.09% on Kodak dataset over VVC when measured in PSNR. Compared with Cheng’20 (Cheng et al. 2020), our MLIC can achieve a maximum improvement of 0.5 ~ 0.8dB in PSNR and achieve a maximum improvement of 0.6dB in MS-SSIM on Kodak, our MLIC⁺ can achieve a maximum improvement of 0.8 ~ 1.0dB in PSNR. Our MLIC and MLIC⁺ are based on Cheng’20 (Cheng et al. 2020) and we remove attention modules and GMM, therefore, the improvement of model performance is attributed to our Multi-Reference Entropy Models. Our Multi-Reference Entropy Models can capture more contexts. We illustrate the amount of contexts captured by different entropy models in our supplementary material. The improvement also proves correlations exist in multiple dimensions since Cheng’20 (Cheng et al. 2020) adopts an spatial autoregressive context model. Compared with ELIC (He et al. 2022), our MLIC⁺ can be up to 0.4db higher at low bit rate and reduce BD-rate by 6.23% over ELIC (He et al. 2022). Our MLIC and MLIC⁺ have a slight performance degradation at the last bit rate, which can be attributed to less channels of MLIC and weaker analysis and synthesis transform. ELIC (He et al. 2022) adopts stacked residual bottlenecks and attention blocks, which makes analysis transform g_a and synthesis transform g_s deeper than ours and has better non-linearity.

Qualitative Results Figure 12 illustrates the example of reconstructed Kodim07 of our MLIC, our MLIC⁺, Entroformer (Qian et al. 2022), Xie’21 (Xie, Cheng, and Chen 2021), Cheng’20 (Cheng et al. 2020) and VTM17.0 (JVET 2021). PSNR value of our reconstructed images are 1dB higher than image reconstructed by VTM17.0. Our reconstructed images retain more details with lower bpp. In terms of visual quality, our MLIC and MLIC⁺ have significant

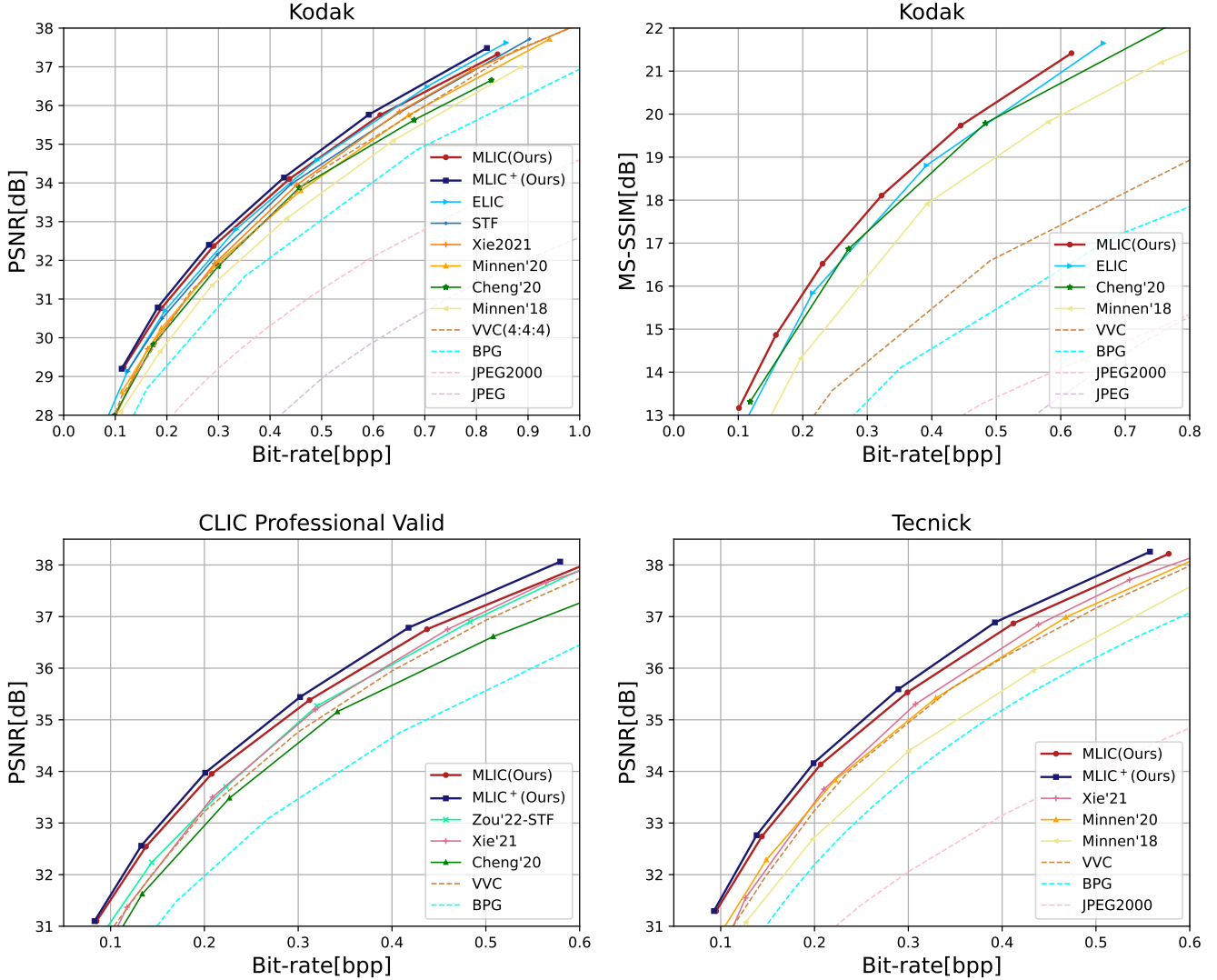


Figure 11: PSNR-Bit-rate curve on Kodak, CLIC Professional Valid dataset and Tecnick (Asuni and Giachetti 2014) (opt. MSE) and MS-SSIM-Bit-rate curve on Kodak dataset (opt. MS-SSIM). Please refer to our supplementary material for rate-distortion performance on CLIC2021-Test and JPEGAI Test (JPEG-AI 2020) dataset. The authors of ELIC (He et al. 2022) mistyped CLIC 2021 Test dataset as CLIC Professional Valid dataset, so there is no RD data of ELIC (He et al. 2022) on CLIC Professional Valid dataset. We confirmed this via email.

	<i>glc,ar</i>	<i>glc,stk</i>	<i>glc,attn</i>	<i>gch</i>	<i>ggc,intra</i>	<i>ggc,inter</i>
Case 1	✓					
Case 2		✓				
Case 3			✓			
Case 4		✓		✓		
Case 5		✓		✓	✓	
Case 6		✓		✓	✓	✓

Table 4: The specific configuration of ablation studies.

improvements compared to other models. We provide more qualitative results in our supplementary material.

Codec Efficiency Analysis Spatial auto-regressive context capturing is effective while leading to serial decoding. GMM can perform more flexible probability estimation but requires additional calculation of CDFs and PDFs. Therefore, we do not adopt them in our model. Although we divide \hat{y} into slices, since MLIC has only 6 slices and MLIC+ has only 10 slices and the resolution of each slice is small, the serial processing between slices does not add too much time. We compare our MLIC and MLIC+ with other classic models on encoding latency, decoding latency and forward



Figure 12: Visualization of the reconstructed Kodim07 from Kodak dataset. The metrics are [bpp↓/PSNR↑]. We compare our MLIC and MLIC⁺ with Cheng’20 (Cheng et al. 2020), Xie’21 (Xie, Cheng, and Chen 2021), Entroformer (Qian et al. 2022) and VTM17.0 (JVET 2021).

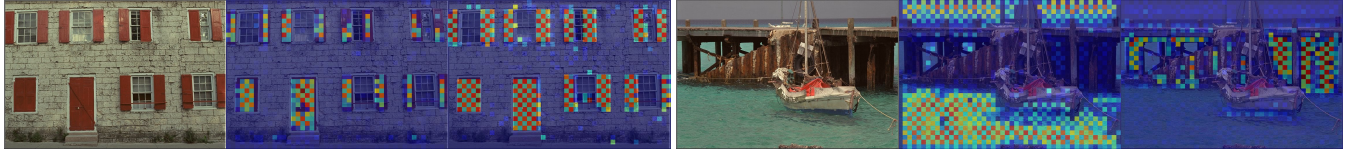


Figure 13: Attention map of Kodim01 and Kodim11 extracted by Intra-Global Context Model of MLIC (optimized for MSE, $\lambda = 0.0035$). Because interactions within anchor and nonanchor part are not allowed, the attention map is checkerboard-like.

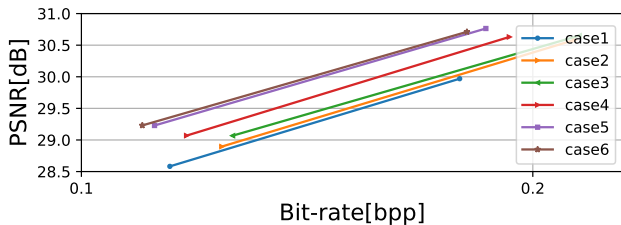


Figure 14: Ablation Studies on Kodak dataset.

Flops, which are illustrated in Table 3. We use Cheng’20 (Cheng et al. 2020) with checkerboard context model (He et al. 2021) as anchor. Compared with anchor, the decoding latencies of our MLIC and MLIC⁺ do not increase much. Compared with Cheng’20 (Cheng et al. 2020), our MLIC achieves much better rate-distortion performance with similar Flops. It takes much less time for our MLIC and MLIC⁺ to decode an image.

Ablation Studies

We conduct corresponding ablation studies on Kodak dataset to evaluate the contributions of proposed entropy models. The results and configure are shown in Figure 14 and Table 4, respectively.

Analysis of Channel Fusion Module The gain of channel fusion module is predictable because it makes it possible to refer to symbols in the same position in the previous slices and refer to more symbols when encoding current slice.

Analysis of Local Context Capturing The checkerboard context model can lead up to 4% performance degradation. Our Stacked Checkerboard Context Module and Checkerboard Attention Module can even outperform the spatial autoregressive context model. One convolutional layer can only capture linear contexts while our models capture non-linear contexts. Non-linearity leads to performance gains.

Analysis of Global Context Capturing We illustrate attention map of Intra-Slice Context Module in Figure 8. Our model successfully captures distant correlations, which are impossible for local context models to capture. Our Intra-Slice Global Context Module may be somewhat similar to the cross-attention model. However, we don’t care about interactions between these two slices. We only use the attention map of \hat{y}^{i-1} to predict correlations in \hat{y}^i . The gain of Inter-Slice Global Context Module is a little small. One problem of our methods for global context is their quadratic computational complexity. One solution is cropping an image into patches. We find cropping an image into non-overlapped patches has almost no influence on performance. The results are reported in our supplementary material. We are investigating shared attention map and learn-able global tokens to reduce complexity while retaining performance.

Conclusion

In this paper, we propose multi-reference entropy models MEM and MEM⁺, which capture correlations in multiple dimensions. To our knowledge, this is the first successful attempt to capture channel, local and global correlations. Based on MEM and MEM⁺, we obtain state-of-the-art model MLIC and MLIC⁺. The significance of our work may be investigating multiple correlations in latent representation and exploring the potential of an entropy model. However, due to the computational overhead, MLIC and MLIC⁺ cannot be directly applied to mobile devices. We expect that this problem can be addressed by using knowledge distillation, network pruning, structural re-parameterization and other light-weight designs.

Acknowledgements

This work is supported by National Natural Science Foundation of China U21B2012, 62072013 and 61902008, Shenzhen Cultivation of Excellent Scientific and Technological Innovation Talents RCJC20200714114435057, Shen-

zhen Research Projects of JCYJ20180503182128089 and
201806080921419290.

A. Context Modeling Comparison

We first illustrate various context models in Figure 15. Our Multi-reference Entropy Model MEM and MEM⁺ can capture more correlations. Spatial context models (Klopp et al. 2018; Minnen, Ballé, and Toderici 2018; Lee, Cho, and Beack 2019; He et al. 2021) adopt the same mask for all channels when extracting contexts, which means there are always some correlations that cannot be captured. For a channel-wise context model (Minnen and Singh 2020), there is no interactions in the current slice. In ELIC (He et al. 2022), the limited receptive field cannot capture correlations between distant symbols. Multi-reference Entropy Model MEM and MEM⁺ consists of three modules: local spatial context module, global spatial context module and channel context module. Based on these modules, our MEM and MEM⁺ can capture more correlations, which boost the performance of our MLIC and MLIC⁺.

B. More Network Architecture Details

When encoding, we split latent representation $\hat{\mathbf{y}}$ into anchor part $\hat{\mathbf{y}}_a^i$ and nonanchor part $\hat{\mathbf{y}}_{na}^i$. The architecture of our Channel Fusion Model is illustrated in Figure 17. The architecture of Stacked Checkerboard Context Model is illustrated in Figure 18, which contains three 5×5 convolutional layers. We use GELU (Hendrycks and Gimpel 2016) to have non-linearity. The architecture of Stacked Checkerboard Context Model is illustrated in Figure 20. The architecture of FFN is illustrated in Figure 19. The architecture of inter-slice global context model is illustrated in Figure 21.

C. Detailed Experiment Settings

We implement our MLIC and MLIC+ on Pytorch 1.10.0 (Paszke et al. 2019), CompressAI 1.2.0b3 (Bégaint et al. 2020) and Python 3.9.7. We use fvcore (MetaResearch 2019) to evaluate FLOPs. We use a Titan X GPU with Maxwell architecture and an Intel i7-7700 cpu on WSL2 to test encoding and decoding latency. We do not enable the deterministic inference mode when testing the model speeds.

D. Experiments on Other Backbone and Simpler Global Context Module

As stated in the main paper, using Cheng'20 (Cheng et al. 2020) without attention modules leads to performance degradation at high bit-rates. We replace it with backbone of ELIC (He et al. 2022). Different from ELIC, we evenly divide the latent representation into slices. We simplify the Intra-Slice Global Context Module by sharing attention maps. We use the attention map of the first slice to predict global correlations in other slices. The process of Intra-Slice Global Context Module can be formulated as:

$$\hat{\mathbf{y}}_{attn}^i = \text{softmax} \left(\frac{\hat{\mathbf{y}}_{na,q}^1 \times (\hat{\mathbf{y}}_{a,k}^1)^\top}{\sqrt{S}} + \text{mask} \right) \times \hat{\mathbf{y}}_{a,v}^i, \quad (15)$$

$$\hat{\mathbf{y}}_{conv}^i = \text{conv}_{K \times K}(\hat{\mathbf{y}}_{attn}^i) + \hat{\mathbf{y}}_{a,v}^i, \quad (16)$$

$$\Phi_{gc,intra}^i = \text{FFN}(\hat{\mathbf{y}}_{conv}^i) + \hat{\mathbf{y}}_{conv}^i, \quad (17)$$

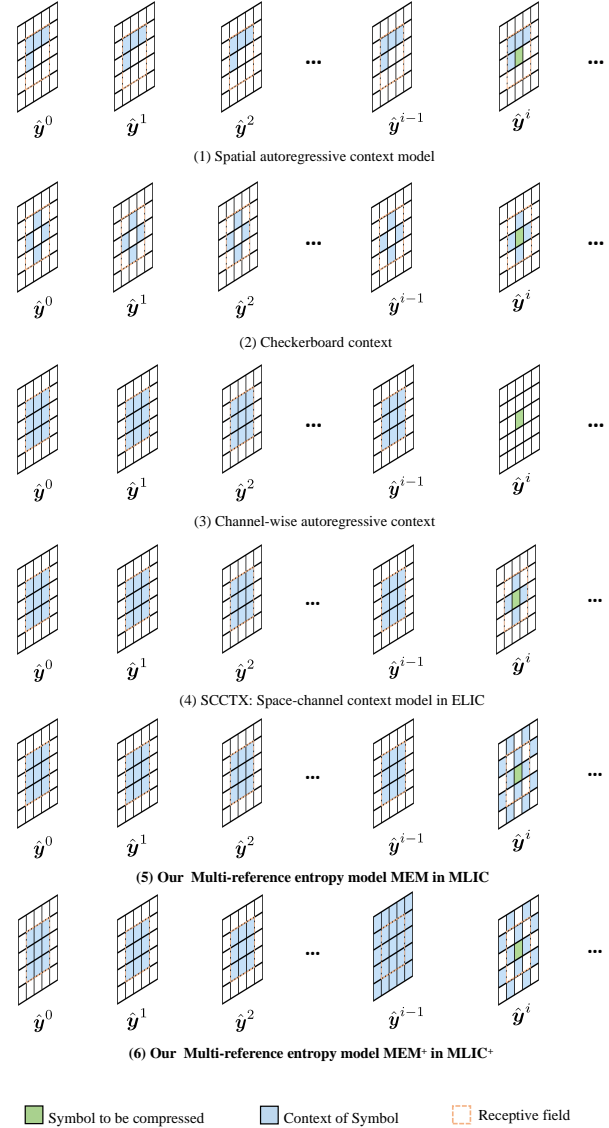


Figure 15: Illustration of various context models. For local context models, we also divide latent representation $\hat{\mathbf{y}}$ into slices $\{\hat{\mathbf{y}}^1, \hat{\mathbf{y}}^2, \hat{\mathbf{y}}^3, \dots\}$. Please zoom in for better view.

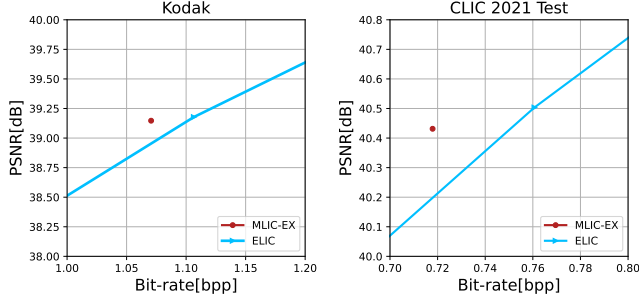


Figure 16: PSNR-Bit-rate curve on Kodak and CLIC 2021 Test dataset.

where $\hat{y}_{na,q}^1, \hat{y}_{a,k}^1 = \text{Embed}(\hat{y}^1)$, $\hat{y}_{a,v}^i = \text{Embed}(\hat{y}_a^i)$. We remove Inter-Slice Global Context Module and Latent Residual Prediction modules (Minnen and Singh 2020) to further reduce complexity. We call this model MLIC-EX, meaning extra version of MLIC. We optimize MLIC-EX for MSE. We set λ to 0.08 to evaluate the performance on high bit-rates. We compare our MLIC-EX on Kodak and CLIC 2021 Test dataset. The performance of MLIC-EX is shown in Figure 16. Although sharing attention maps leads to slight performance drop, our MLIC-EX outperforms ELIC.

E. More Rate-Distortion Performance Results

We illustrate detailed rate-distortion performance in Figure 22, 23, 24, 26, 27, 28.

Kodak dataset is available at <http://r0k.us/graphics/kodak>.

Tecnick dataset is available at https://sourceforge.net/projects/testimages/files/OLD/OLD_SAMPLING/testimages.zip.

CLIC Professional Valid dataset is available at https://data.vision.ee.ethz.ch/cvl/clic/professional_valid_2020.zip.

CLIC2021 Test dataset is available at https://storage.googleapis.com/clic2021_public/professional_test_2021.zip.

JPEGAI Test dataset is available at https://jpegai.github.io/test_images/.

We compare our methods with learned image compression methods Minnen’18 (Minnen, Ballé, and Toderici 2018), Cheng’20 (Cheng et al. 2020), Minnen’20 (Minnen and Singh 2020), Guo’21 (Guo et al. 2021a), Gao’21 (Gao et al. 2021), Xie’21 (Xie, Cheng, and Chen 2021), Entroformer (Qian et al. 2022), STF (Zou, Song, and Zhang 2022), ELIC (He et al. 2022), Contextformer (Koyuncu, Gao, and Steinbach 2022) and traditional image compression methods JPEG (ITU 1992), JPEG2000 (Charrier, Cruz, and Larsson 1999), BPG (Bellard 2015), VTM (JVET 2021).

When evaluating performance on CLIC Professional Valid dataset (Toderici et al. 2020), Tecnick (Asuni and Giachetti 2014) and CLIC2021 Test (Toderici et al. 2020), we pad images to multiples of 64. There are few results on JPEGAI Test. We only compare our MLIC and MLIC⁺ with Xie’21 (Xie, Cheng, and Chen 2021). We obtain rate-distortion data of other models by asking au-

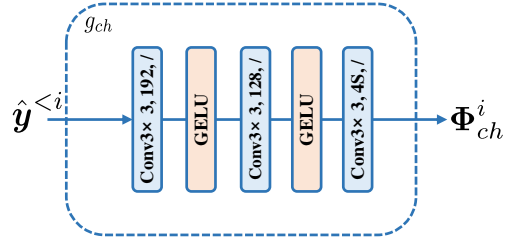


Figure 17: Channel Fusion Module g_{ch} .

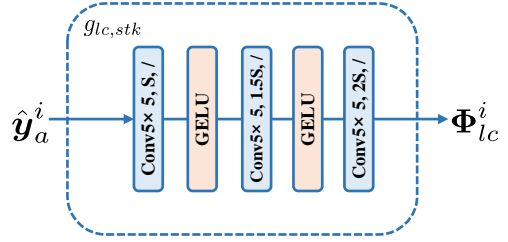


Figure 18: Stacked Checkerboard Context Module $g_{lc,stk}$.

thors via emails. We get the rate-distortion data of VVC (JVET 2021) via commands of CompressAI (Bégaint et al. 2020) from <https://github.com/InterDigitalInc/CompressAI/blob/master/compressai/utis/bench/codecs.py>. We use the code from https://github.com/Anserw/Bjontegaard_metric to calculate bd-rate.

F. More Visualizations

F.1. Visualization of Reconstructed Images

We select some reconstructed images from Kodak (Kodak 1993). We compare our MLIC and MLIC⁺ with Xie’21 (Xie, Cheng, and Chen 2021), Cheng’20 (Cheng et al. 2020) and VTM17.0 (JVET 2021). Please see Figure 29, 30 for reconstructed images.

F.2. Visualization of Attention Maps

To prove the effectiveness of our global context modules, we provide more attention maps in Figure 31, 32, 34, 33.

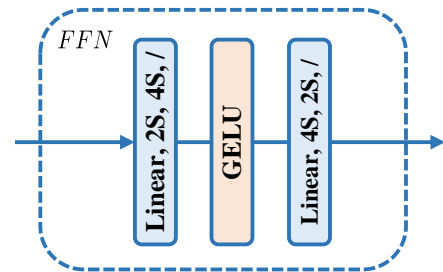


Figure 19: FFN.

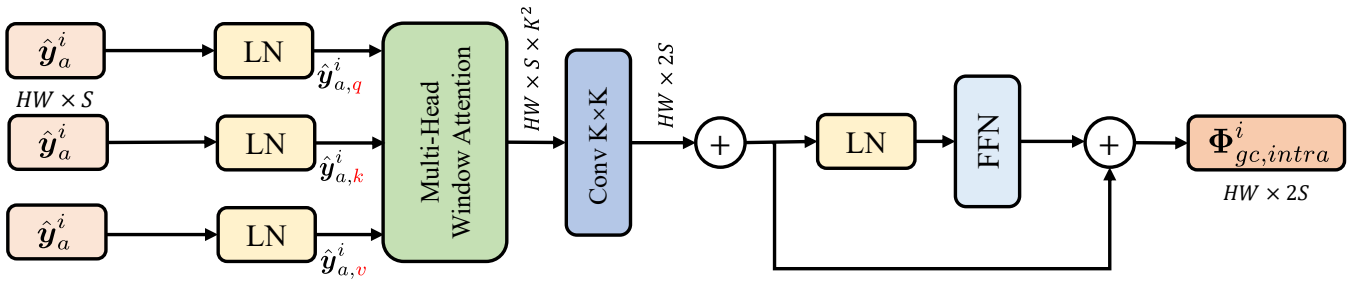


Figure 20: Checkerboard Attention Context Module $g_{lc,attn}$.

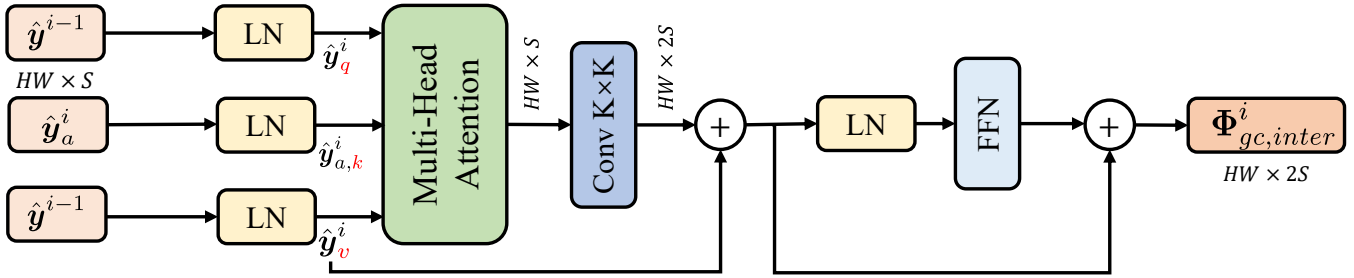


Figure 21: Inter-Slice Global Context Module $g_{gc,inter}$. S is the channel number of a slice.

G. Influence of Resolution

We are interested in the influence of resolution of images. Our intra-slice global context module $g_{gc,intra}$ and inter-slice global context module $g_{gc,inter}$ are based on Transformers (Vaswani et al. 2017). Transformers are not translation invariant, which means there is an inconsistency between training and testing. Another reason is the computational complexity when compressing images with high resolution, which means that we need to crop images with high resolution into patches. We compare our MLIC and MLIC⁺ on CLIC Professional Valid dataset (Toderici et al. 2020). We crop images into non-overlapped 448×448 patches. To avoid the influence of padding zeros, all images are cropped to multiples of 448. The results in illustrated in Figure 35. When compressing non-overlapped patches, there is almost no performance degradation. Maybe global correlations within 448×448 patch are enough for conditional probability estimation. Figure 36 shows the example of compressing an image and compressing patches.

H. Progressive Decoding Analysis

Learned Image Compression Models with channel-wise context model usually supports progressive decoding (Minnen and Singh 2020; He et al. 2022). We also illustrate the progressive decoding results of our MLIC in Figure 37. However, the progressive decoding performance of MLIC is much worse than the performance of separated optimized models. What's more, we find the performance of progressive decoding is not stable. Sometimes progressive decoding leads to unpleasant anti-facts and noise or crashes. Progressive decoding results of our MLIC⁺ is much worse. The problems can be attributed to our global spatial context

modules. It seems that the inter-slice global context model changes the information distribution between slices. Compared with channel-wise context model, our global context modules are extra constraints.

We think channel-wise context model is a good method for progressive decoding. But when using channel-wise context model, we need to design a suitable method to change the information between slices to optimized the performance (Ma, Zhai, and Wang 2022).

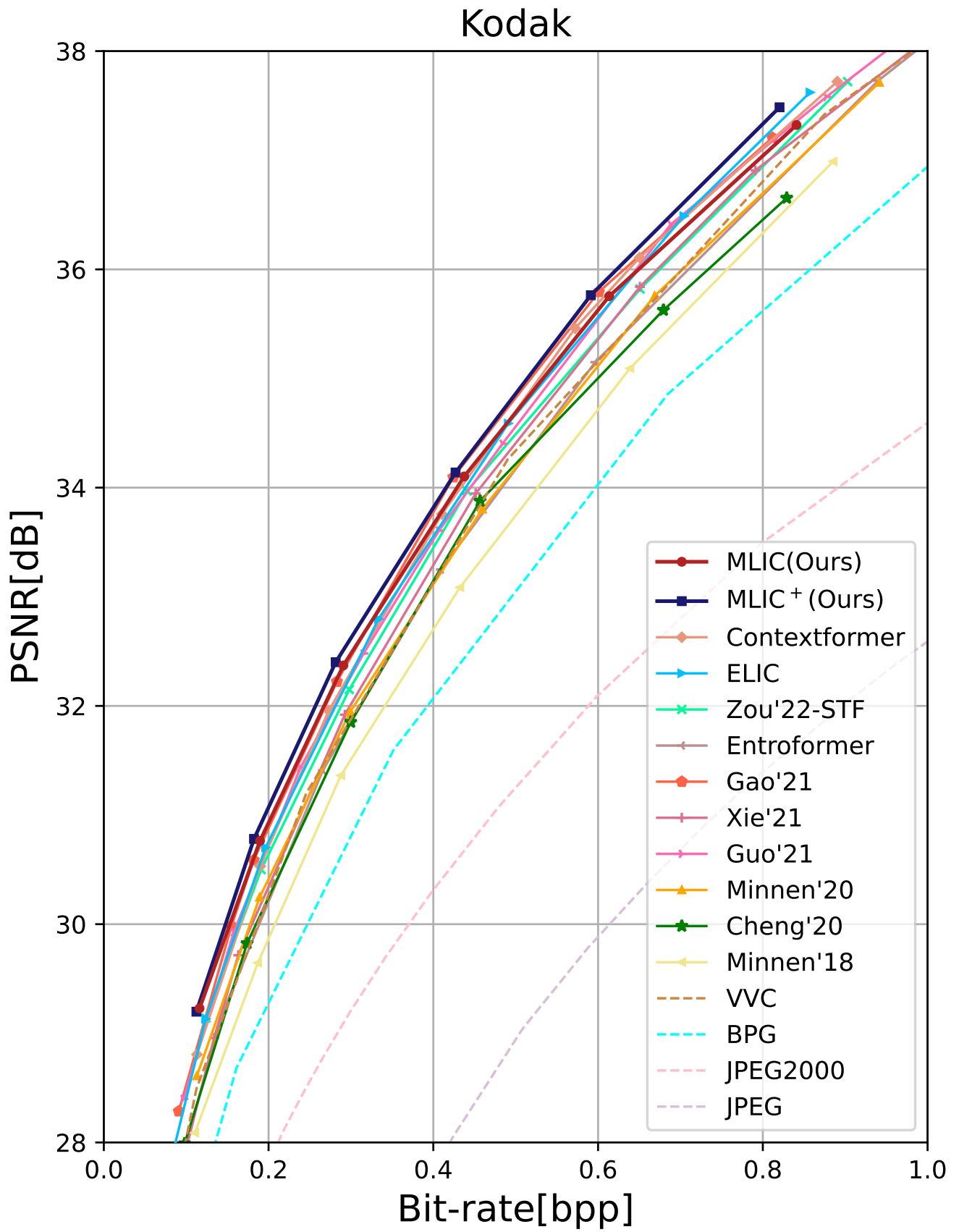


Figure 22: Rate-distortion data of MLIC and MLIC+ on Kodak dataset, which contains 24 raw images.

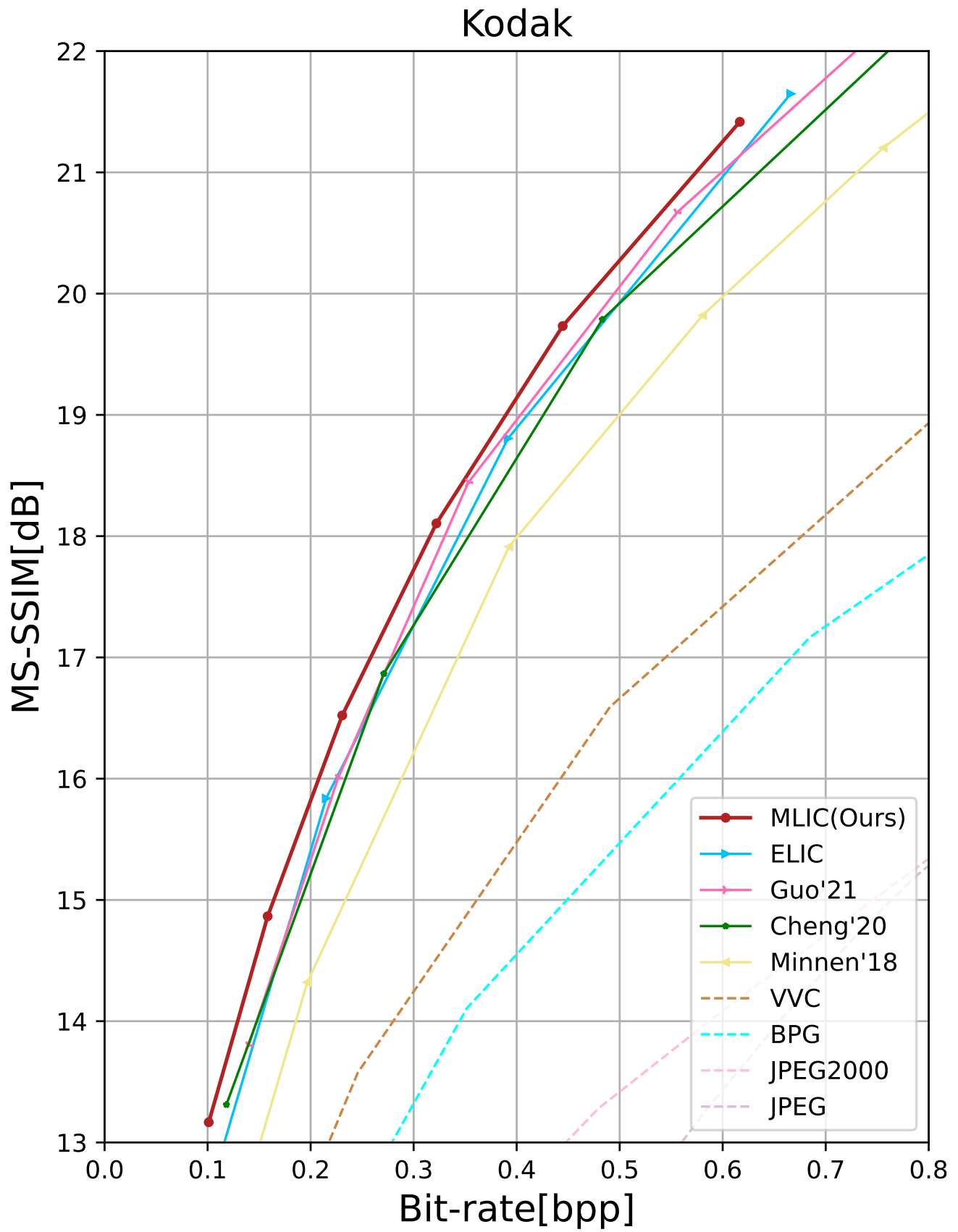


Figure 23: Rate-distortion data of MLIC on Kodak dataset, which contains 24 raw images.

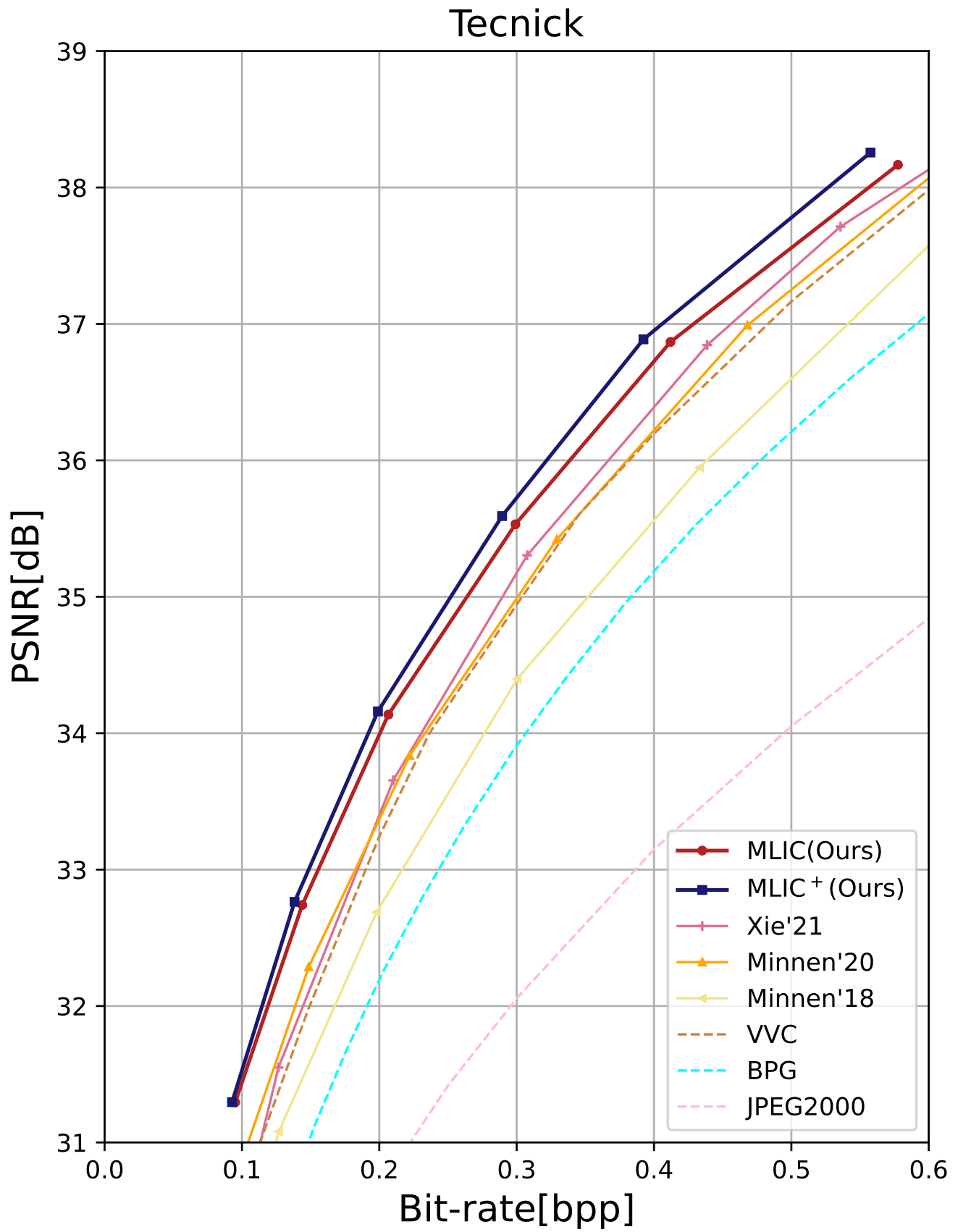


Figure 24: Rate-distortion data of MLIC and MLIC+ on Tecnick dataset, which contains 100 raw images. All images are padded to multiples of 64.

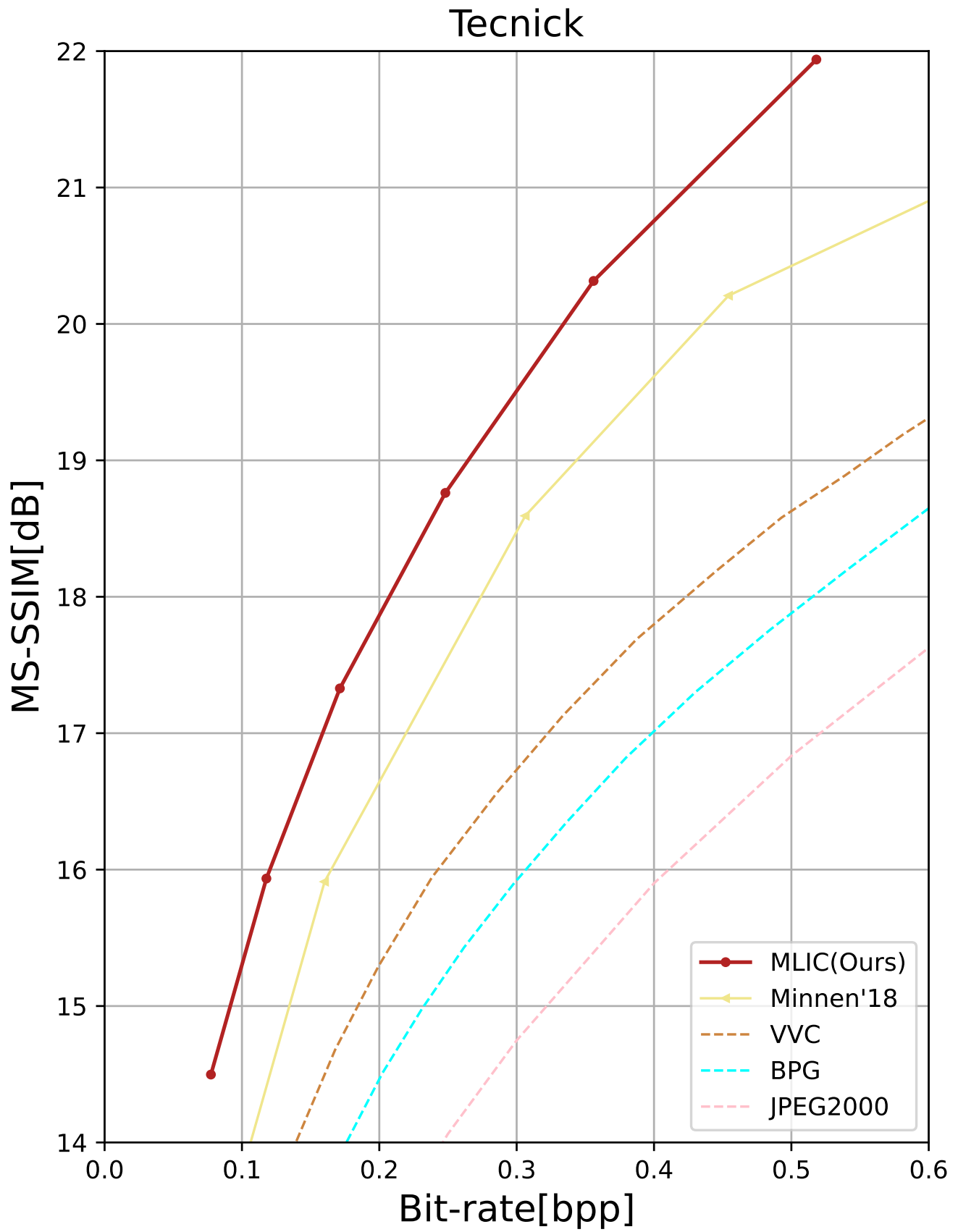


Figure 25: Rate-distortion data of MLIC and MLIC+ on Tecnick dataset, which contains 100 raw images. All images are padded to multiples of 64.

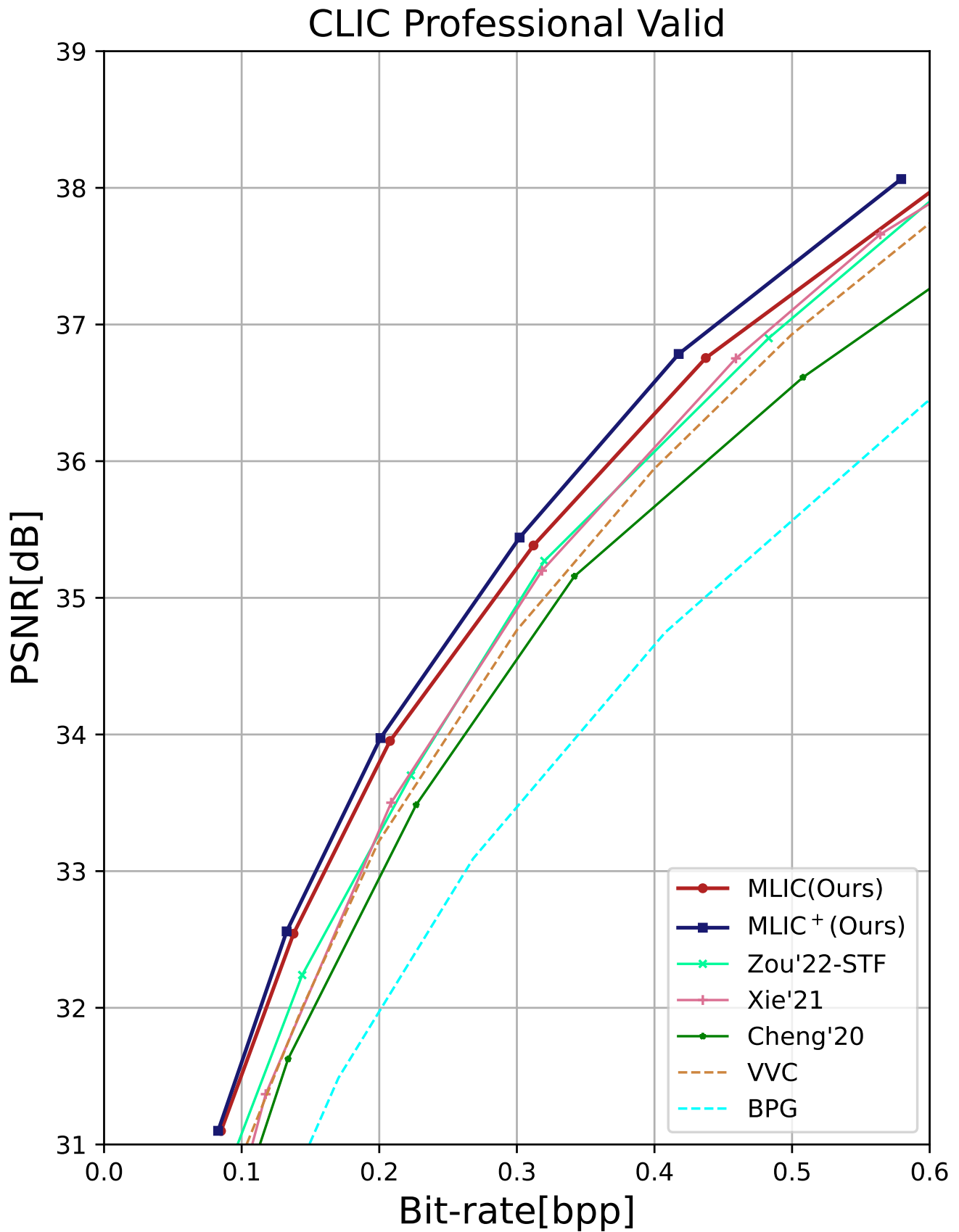


Figure 26: Rate-distortion data of MLIC and MLIC+ on CLIC Professional Valid dataset, which contains 41 raw images. All images are padded to multiples of 64.

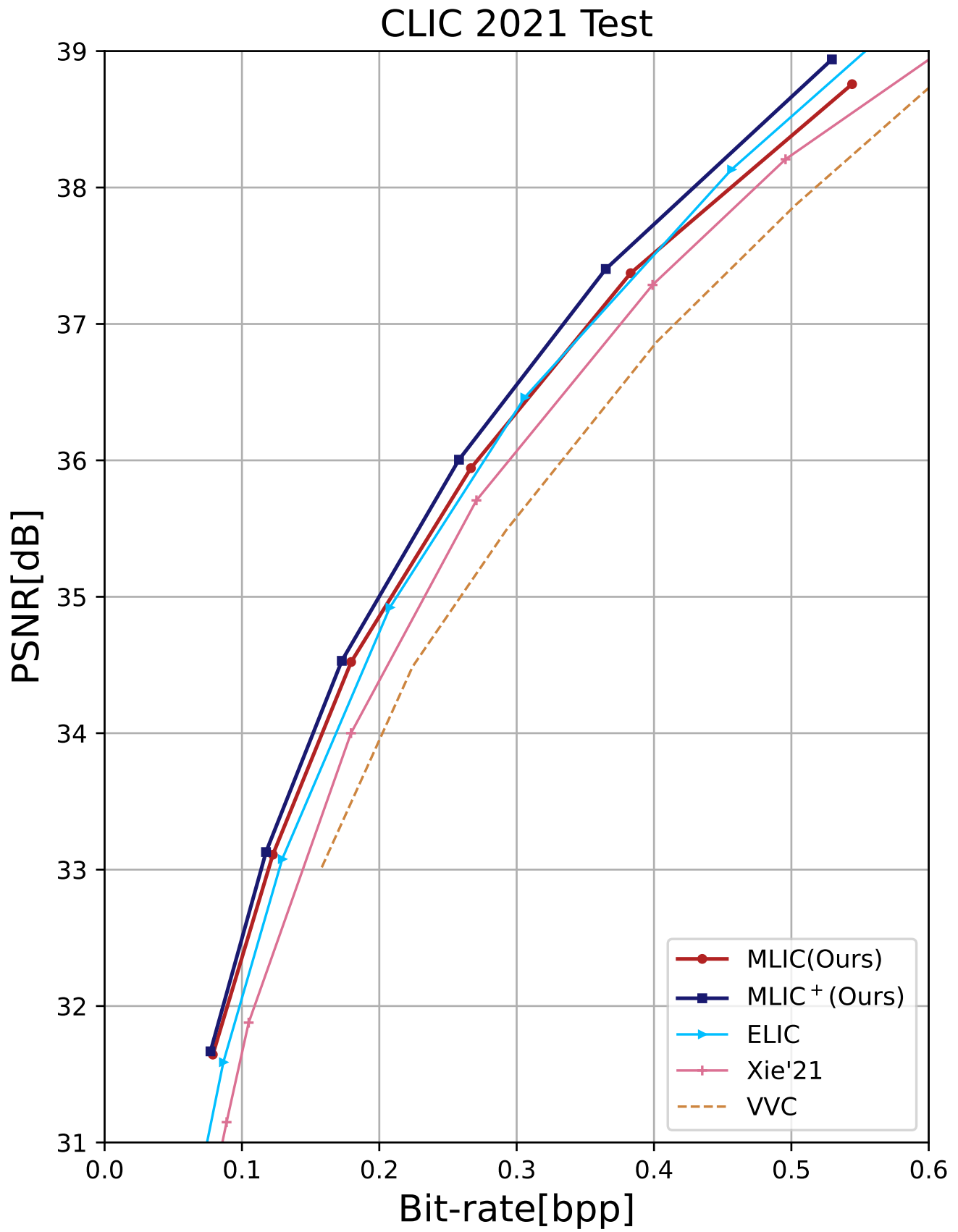


Figure 27: Rate-distortion data of MLIC and MLIC+ on CLIC 2021 Test dataset, which contains 60 raw images. All images are padded to multiples of 64.

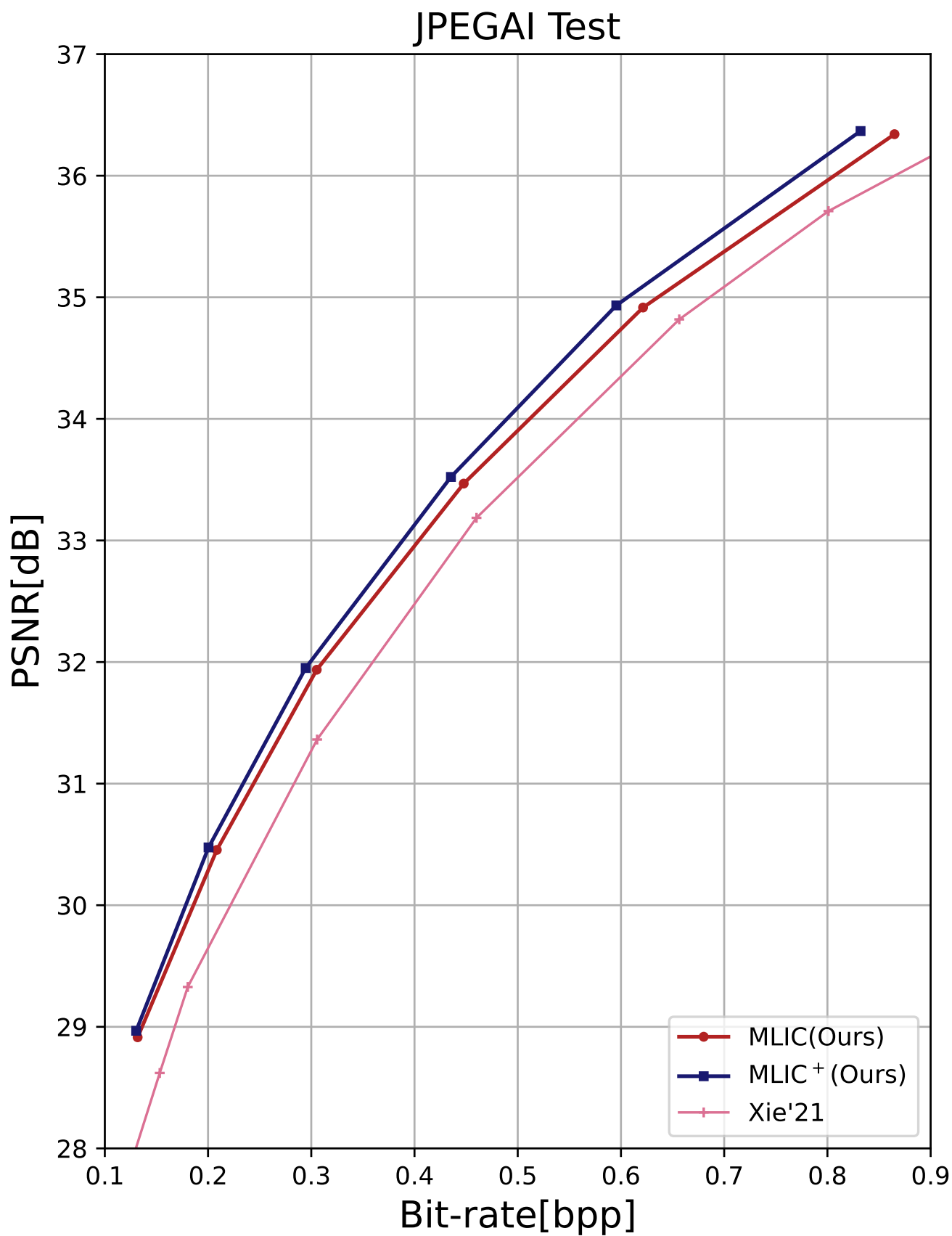


Figure 28: Rate-distortion data of MLIC and MLIC+ on JPEGAI Test dataset, which contains 12 raw images. All images are padded to multiples of 64.

Original



Bpp / PSNR

Cheng'20



0.1227 / 30.9514

Xie'21



0.1134 / 30.8153

VTM17.0



0.1321 / 31.1412

MLIC



0.1344 / 32.0555

MLIC+



0.1305 / 32.0212

Figure 29: Qualitative comparison on reconstructed kodim17. The metrics are [bpp↓/PSNR↑].

Original



Bpp / PSNR

Xie'21



0.1152 / 29.6897

MLIC



0.1347 / 30.5968

Cheng'20



0.1339 / 29.6726

VTM17.0



0.1291 / 29.9380

MLIC+



0.1269 / 30.5905

Figure 30: Qualitative comparison on reconstructed kodim19. The metrics are [bpp↓/PSNR↑].



Kodim15

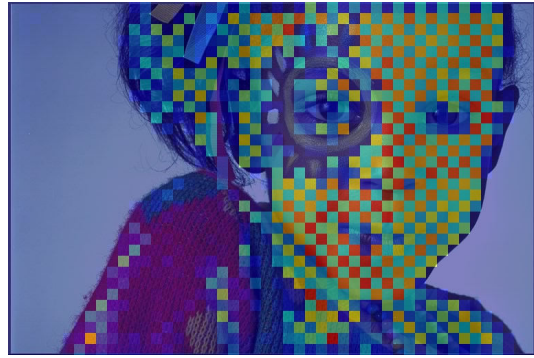


Figure 31: Attention map of Intra-Slice Global Context Model of MLIC(optimized for MSE, $\lambda = 0.0035$). Because we divide latent representation into anchor and non-anchor, the attention map is checkerboard-like.



Kodim20



Figure 32: Attention map of Intra-Slice Global Context Model of MLIC(optimized for MSE, $\lambda = 0.0035$). Because we divide latent representation into anchor and non-anchor, the attention map is checkerboard-like.



RGB_OR_1200x1200_031

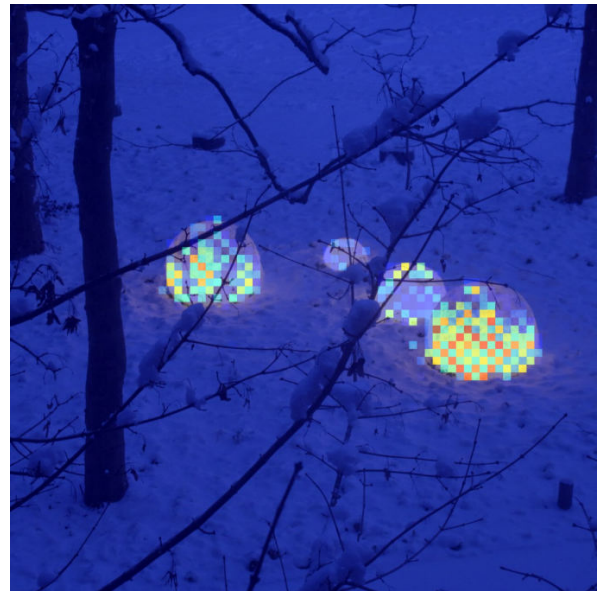
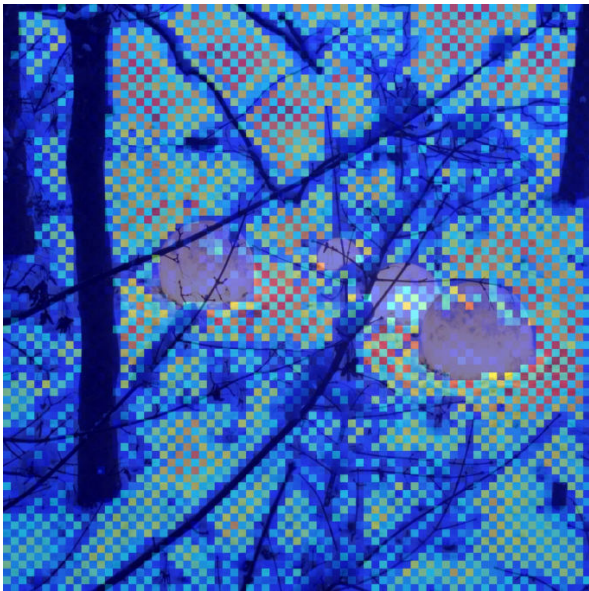
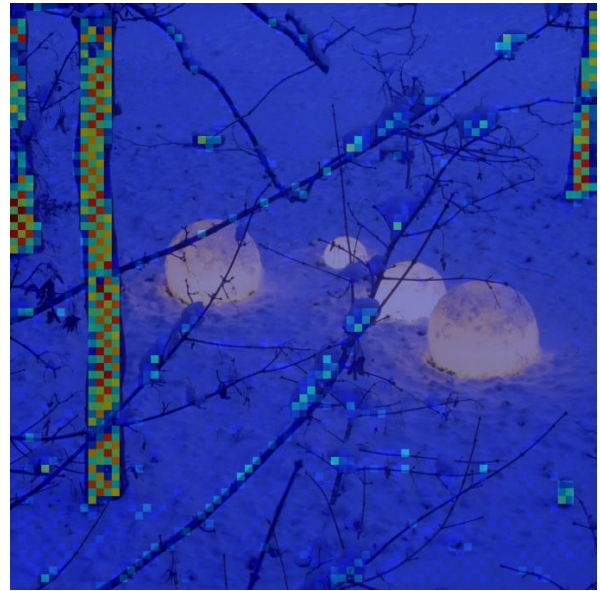
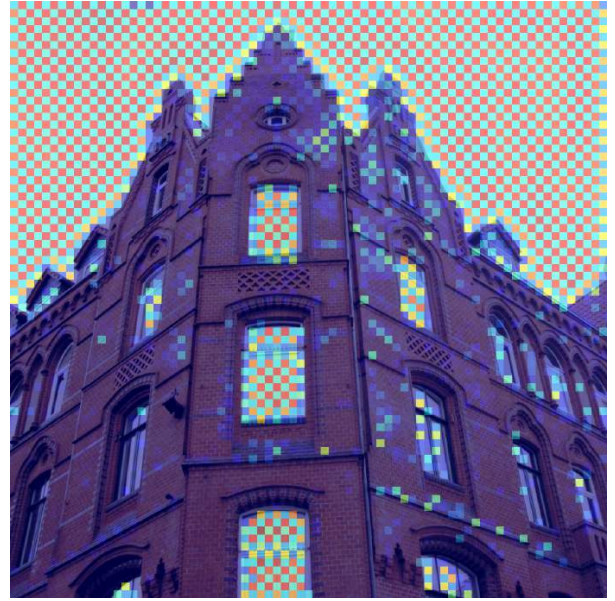


Figure 33: Attention map of Intra-Slice Global Context Model of MLIC(optimized for MSE, $\lambda = 0.0035$). Because we divide latent representation into anchor and non-anchor, the attention map is checkerboard-like.



RGB_OR_1200x1200_031

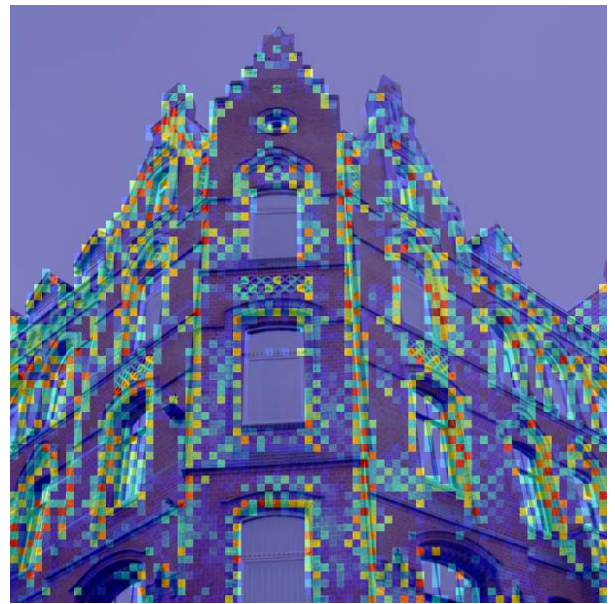


Figure 34: Attention map of Intra-Slice Global Context Model of MLIC(optimized for MSE, $\lambda = 0.0035$). Because we divide latent representation into anchor and non-anchor, the attention map is checkerboard-like.

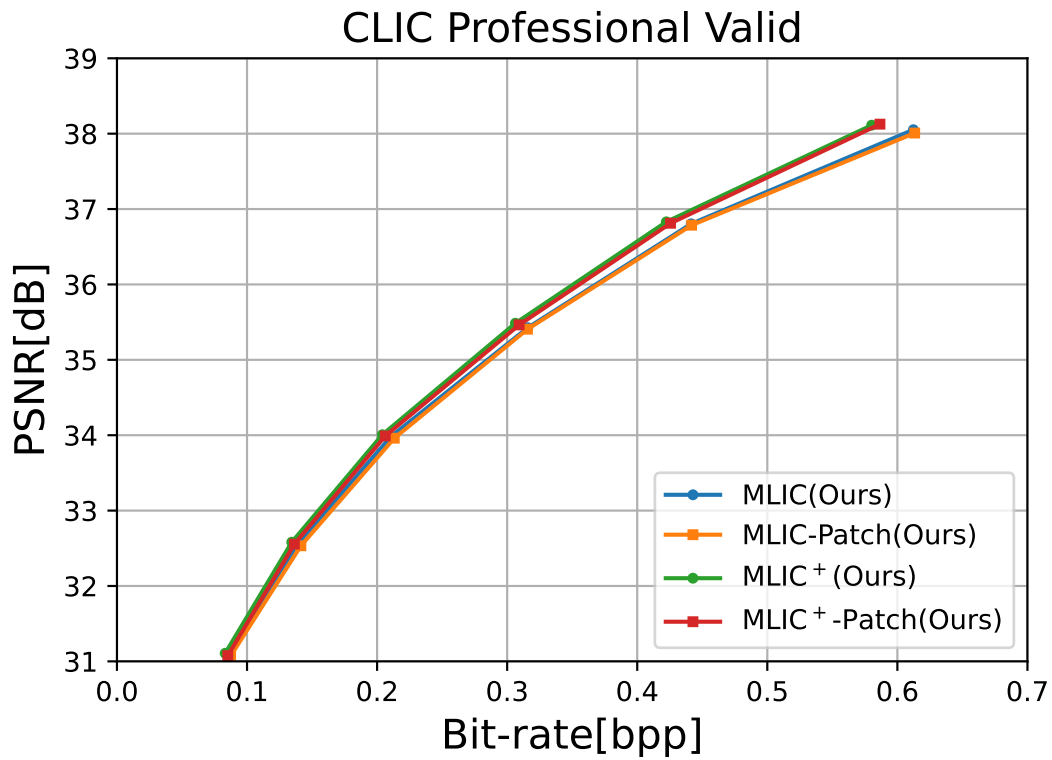


Figure 35: Rate-distortion performance comparison between compressing an image and compressing non-overlapped patches. We evaluate performance on CLIC-Professional Valid dataset. The size of every patch is 448×448 .

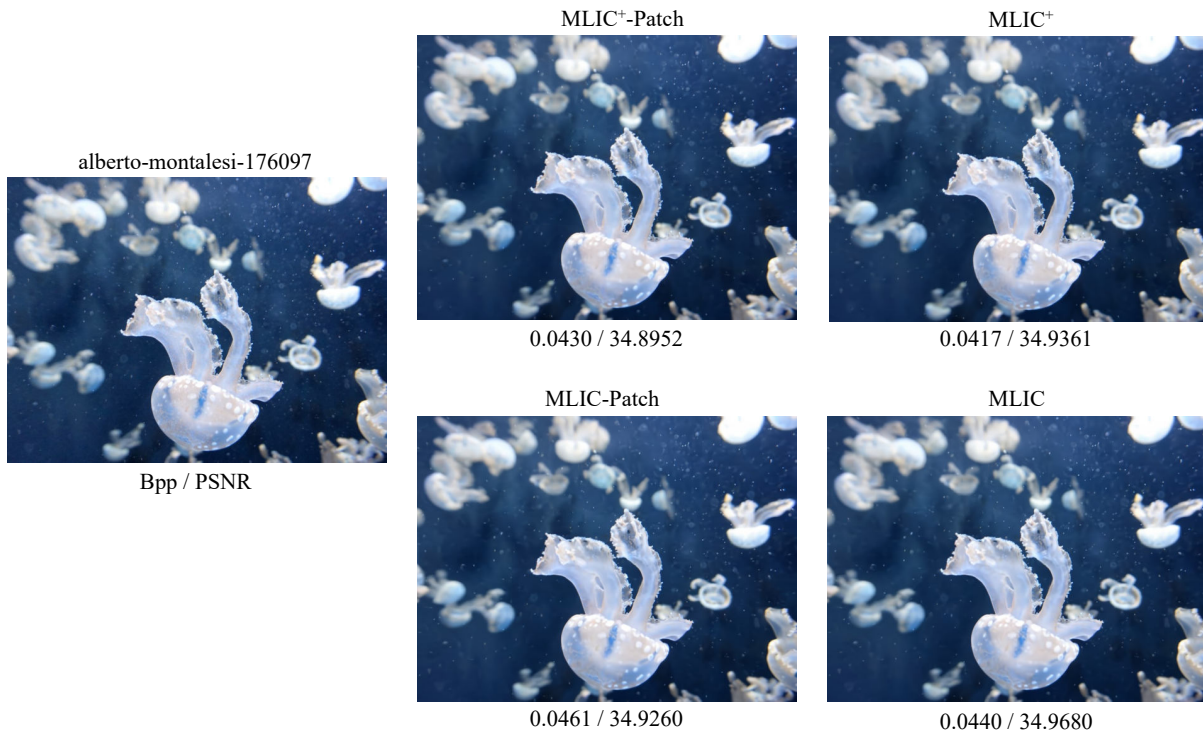


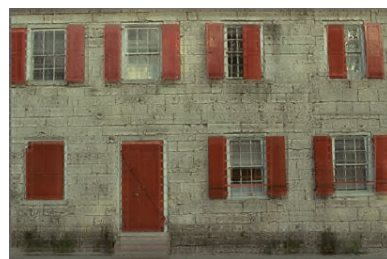
Figure 36: Visualization of the reconstructed image alberto-montalesi-176097. The metrics are [bpp↓/PSNR↑].



Original Kodim01



Slice1-3



Slice1-4



Slice1-5



Slice1-6



Original Kodim04



Slice1-3



Slice1-4



Slice1-5



Slice1-6



Original Kodim21



Slice1-3



Slice1-4



Slice1-5



Slice1-6

Figure 37: Progressive Decoding Results of MLIC on Kodak dataset. We pad latent representation with zeros.

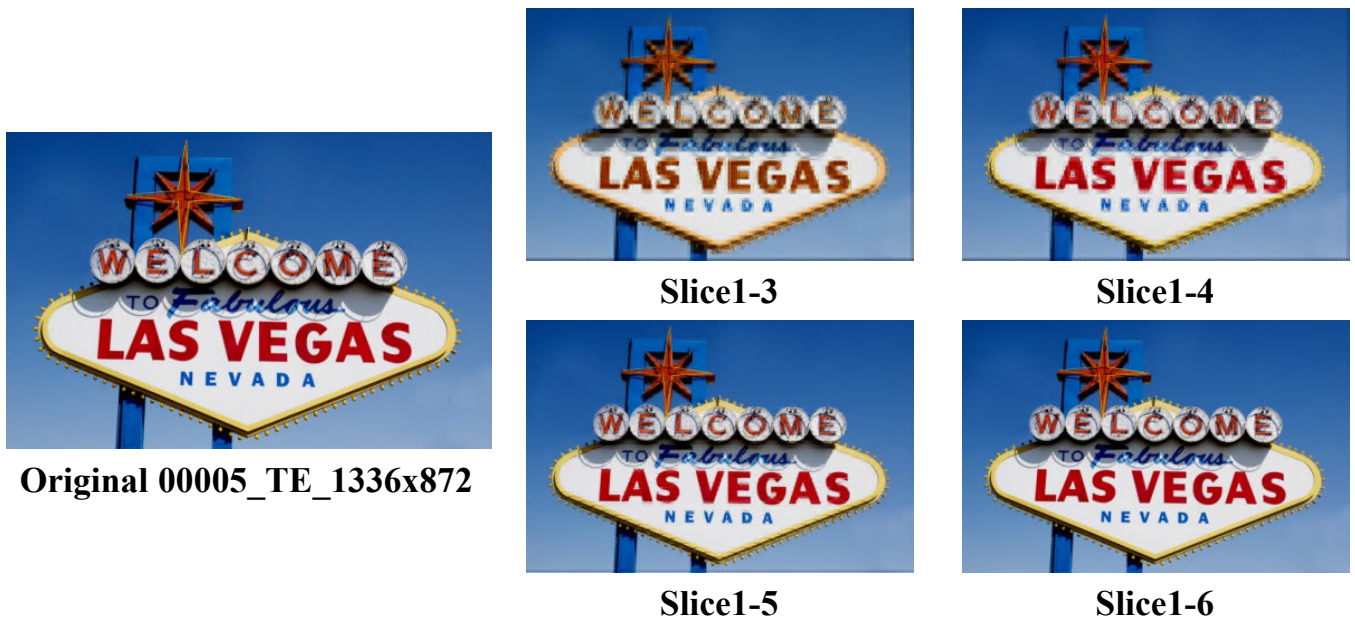


Figure 38: Progressive Decoding Results of MLIC on JPEGAI Test dataset. We pad latent representation with zeros.



Figure 39: Examples of crashed progressive decoding. We pad latent representation with zeros.

References

- Agustsson, E.; and Timofte, R. 2017. NTIRE 2017 Challenge on Single Image Super-Resolution: Dataset and Study. In *Proceedings of the IEEE Conference on Computer Vision and Pattern Recognition (CVPR) Workshops*.
- Akbari, M.; Liang, J.; Han, J.; and Tu, C. 2021. Learned Bi-Resolution Image Coding using Generalized Octave Convolutions. In *Proceedings of the AAAI Conference on Artificial Intelligence*, volume 35, 6592–6599.
- Asuni, N.; and Giachetti, A. 2014. TESTIMAGES: a Large-scale Archive for Testing Visual Devices and Basic Image Processing Algorithms. In *STAG*, 63–70.
- Ayzik, S.; and Avidan, S. 2020. Deep image compression using decoder side information. In *Proceedings of European Conference on Computer Vision*, 699–714. Springer.
- Ballé, J.; Laparra, V.; and Simoncelli, E. P. 2016. Density modeling of images using a generalized normalization transformation. In *International Conference on Learning Representations*.
- Ballé, J.; Laparra, V.; and Simoncelli, E. P. 2017. End-to-end optimized image compression. In *International Conference on Learning Representations*.
- Ballé, J.; Minnen, D.; Singh, S.; Hwang, S. J.; and Johnston, N. 2018. Variational image compression with a scale hyperprior. In *International Conference on Learning Representations*.
- Bégaint, J.; Racapé, F.; Feltman, S.; and Pushparaja, A. 2020. CompressAI: a PyTorch library and evaluation platform for end-to-end compression research. *arXiv preprint arXiv:2011.03029*.
- Bellard, F. 2015. BPG Image format. <https://bellard.org/bpg>.
- Charrier, M.; Cruz, D. S.; and Larsson, M. 1999. JPEG2000, the Next Millennium Compression Standard for Still Images. In *IEEE International Conference on Multimedia Computing and Systems, ICMCS 1999, Florence, Italy, June 7-11, 1999. Volume I*, 131–132. IEEE Computer Society.
- Chen, F.; Xu, Y.; and Wang, L. 2022. Two-Stage Octave Residual Network for End-to-end Image Compression. In *Proceedings of the AAAI Conference on Artificial Intelligence*, volume 36, 3922–3929.
- Chen, T.; Liu, H.; Ma, Z.; Shen, Q.; Cao, X.; and Wang, Y. 2021. End-to-End Learnt Image Compression via Non-Local Attention Optimization and Improved Context Modeling. *IEEE Transactions on Image Processing*, 30: 3179–3191.
- Cheng, Z.; Sun, H.; Takeuchi, M.; and Katto, J. 2020. Learned Image Compression With Discretized Gaussian Mixture Likelihoods and Attention Modules. In *Proceedings of the IEEE/CVF Conference on Computer Vision and Pattern Recognition (CVPR)*.
- Cui, Z.; Wang, J.; Gao, S.; Guo, T.; Feng, Y.; and Bai, B. 2021. Asymmetric Gained Deep Image Compression With Continuous Rate Adaptation. In *Proceedings of the IEEE/CVF Conference on Computer Vision and Pattern Recognition (CVPR)*, 10532–10541.
- Gao, G.; You, P.; Pan, R.; Han, S.; Zhang, Y.; Dai, Y.; and Lee, H. 2021. Neural Image Compression via Attentional Multi-Scale Back Projection and Frequency Decomposition. In *Proceedings of the IEEE/CVF International Conference on Computer Vision*, 14677–14686.
- Guo, Z.; Zhang, Z.; Feng, R.; and Chen, Z. 2021a. Causal Contextual Prediction for Learned Image Compression. *IEEE Transactions on Circuits and Systems for Video Technology*.
- Guo, Z.; Zhang, Z.; Feng, R.; and Chen, Z. 2021b. Soft then hard: Rethinking the quantization in neural image compression. In *International Conference on Machine Learning*, 3920–3929. PMLR.
- He, D.; Yang, Z.; Peng, W.; Ma, R.; Qin, H.; and Wang, Y. 2022. ELIC: Efficient Learned Image Compression With Unevenly Grouped Space-Channel Contextual Adaptive Coding. In *Proceedings of the IEEE/CVF Conference on Computer Vision and Pattern Recognition (CVPR)*, 5718–5727.
- He, D.; Zheng, Y.; Sun, B.; Wang, Y.; and Qin, H. 2021. Checkerboard Context Model for Efficient Learned Image Compression. In *Proceedings of the IEEE/CVF Conference on Computer Vision and Pattern Recognition (CVPR)*, 14771–14780.
- He, K.; Zhang, X.; Ren, S.; and Sun, J. 2016. Deep residual learning for image recognition. In *Proceedings of the IEEE conference on computer vision and pattern recognition*, 770–778.
- Hendrycks, D.; and Gimpel, K. 2016. Gaussian error linear units (gelus). *arXiv preprint arXiv:1606.08415*.
- Hu, Y.; Yang, W.; and Liu, J. 2020. Coarse-to-fine hyperprior modeling for learned image compression. In *Proceedings of the AAAI Conference on Artificial Intelligence*, volume 34, 11013–11020.
- ITU. 1992. Information technology - Digital compression and coding of continuous - tone still images - requirements and guidelines. *CCITT, Recommendation*.
- Johnston, N.; Vincent, D.; Minnen, D.; Covell, M.; Singh, S.; Chinen, T.; Hwang, S. J.; Shor, J.; and Toderici, G. 2018. Improved Lossy Image Compression With Priming and Spatially Adaptive Bit Rates for Recurrent Networks. In *Proceedings of the IEEE Conference on Computer Vision and Pattern Recognition (CVPR)*.
- JPEG-AI. 2020. JPEG-AI Test Images. https://jpegai.github.io/test_images/.
- JVET. 2021. Versatile video coding reference software version 12.1 (VTM-12.1). https://vcgit.hhi.fraunhofer.de/jvet/VVCSoftware_VTM/-/tags/VTM-12.1.
- Kim, J.-H.; Heo, B.; and Lee, J.-S. 2022. Joint Global and Local Hierarchical Priors for Learned Image Compression. In *Proceedings of the IEEE/CVF Conference on Computer Vision and Pattern Recognition (CVPR)*, 5992–6001.
- Kingma, D. P.; and Welling, M. 2014. Auto-Encoding Variational Bayes. In *International Conference on Learning Representations*.

- Klopp, J.; Wang, Y.-C. F.; Chien, S.-Y.; and Chen, L.-G. 2018. Learning a Code-Space Predictor by Exploiting Intra-Image-Dependencies. In *BMVC*, 124.
- Kodak, E. 1993. Kodak lossless true color image suite (PhotoCD PCD0992). <http://r0k.us/graphics/kodak>.
- Koyuncu, A. B.; Gao, H.; and Steinbach, E. 2022. Contextformer: A Transformer with Spatio-Channel Attention for Context Modeling in Learned Image Compression. *arXiv preprint arXiv:2203.02452*.
- Lee, J.; Cho, S.; and Beack, S.-K. 2019. Context-adaptive entropy model for end-to-end optimized image compression. In *International Conference on Learning Representations*.
- Li, M.; Ma, K.; You, J.; Zhang, D.; and Zuo, W. 2020. Efficient and Effective Context-Based Convolutional Entropy Modeling for Image Compression. *IEEE Transactions on Image Processing*, 29: 5900–5911.
- Li, M.; Zuo, W.; Gu, S.; Zhao, D.; and Zhang, D. 2018. Learning convolutional networks for content-weighted image compression. In *Proceedings of the IEEE Conference on Computer Vision and Pattern Recognition*, 3214–3223.
- Lin, C.; Yao, J.; Chen, F.; and Wang, L. 2020. A Spatial RNN Codec for End-to-End Image Compression. In *Proceedings of the IEEE/CVF Conference on Computer Vision and Pattern Recognition*, 13269–13277.
- Lin, T.-Y.; Maire, M.; Belongie, S.; Hays, J.; Perona, P.; Ramanan, D.; Dollár, P.; and Zitnick, C. L. 2014. Microsoft coco: Common objects in context. In *European conference on computer vision*, 740–755. Springer.
- Liu, J.; Lu, G.; Hu, Z.; and Xu, D. 2020. A unified end-to-end framework for efficient deep image compression. *arXiv preprint arXiv:2002.03370*.
- Liu, Z.; Lin, Y.; Cao, Y.; Hu, H.; Wei, Y.; Zhang, Z.; Lin, S.; and Guo, B. 2021. Swin Transformer: Hierarchical Vision Transformer Using Shifted Windows. In *Proceedings of the IEEE/CVF International Conference on Computer Vision (ICCV)*, 10012–10022.
- Lu, M.; Guo, P.; Shi, H.; Cao, C.; and Ma, Z. 2022. Transformer-based Image Compression. In *Data Compression Conference (DCC)*, 469–469.
- Ma, C.; Wang, Z.; Liao, R.; and Ye, Y. 2021. A Cross Channel Context Model for Latents in Deep Image Compression. *arXiv preprint arXiv:2103.02884*.
- Ma, H.; Liu, D.; Yan, N.; Li, H.; and Wu, F. 2020. End-to-end optimized versatile image compression with wavelet-like transform. *IEEE Transactions on Pattern Analysis and Machine Intelligence*.
- Ma, Y.; Zhai, Y.; and Wang, R. 2022. DeepFGS: Fine-Grained Scalable Coding for Learned Image Compression. *arXiv preprint arXiv:2201.01173*.
- Mentzer, F.; Agustsson, E.; Tschannen, M.; Timofte, R.; and Van Gool, L. 2018. Conditional probability models for deep image compression. In *Proceedings of the IEEE Conference on Computer Vision and Pattern Recognition*, 4394–4402.
- Metaresearch. 2019. fvccore. <https://github.com/facebookresearch/fvccore>.
- Minnen, D.; Ballé, J.; and Toderici, G. D. 2018. Joint autoregressive and hierarchical priors for learned image compression. In *Advances in Neural Information Processing Systems*, 10771–10780.
- Minnen, D.; and Singh, S. 2020. Channel-wise autoregressive entropy models for learned image compression. In *2020 IEEE International Conference on Image Processing (ICIP)*, 3339–3343. IEEE.
- Paszke, A.; Gross, S.; Massa, F.; Lerer, A.; Bradbury, J.; Chanan, G.; Killeen, T.; Lin, Z.; Gimelshein, N.; Antiga, L.; et al. 2019. Pytorch: An imperative style, high-performance deep learning library. *Advances in neural information processing systems*, 32.
- Pennebaker, W. B.; and Mitchell, J. L. 1992. *JPEG: Still image data compression standard*. Springer Science & Business Media.
- Qian, Y.; Lin, M.; Sun, X.; Tan, Z.; and Jin, R. 2022. Entroformer: A Transformer-based Entropy Model for Learned Image Compression. In *International Conference on Learning Representations*.
- Qian, Y.; Tan, Z.; Sun, X.; Lin, M.; Li, D.; Sun, Z.; Li, H.; and Jin, R. 2021. Learning Accurate Entropy Model with Global Reference for Image Compression. In *International Conference on Learning Representations*.
- Rippel, O.; and Bourdev, L. 2017. Real-time adaptive image compression. In *Proceedings of the 34th International Conference on Machine Learning-Volume 70*, 2922–2930. JMLR. org.
- Russakovsky, O.; Deng, J.; Su, H.; Krause, J.; Satheesh, S.; Ma, S.; Huang, Z.; Karpathy, A.; Khosla, A.; Bernstein, M.; Berg, A. C.; and Fei-Fei, L. 2015. ImageNet Large Scale Visual Recognition Challenge. *International Journal of Computer Vision (IJCV)*, 115(3): 211–252.
- Theis, L.; Shi, W.; Cunningham, A.; and Huszár, F. 2017. Lossy image compression with compressive autoencoders. In *International Conference on Learning Representations*.
- Toderici, G.; O’Malley, S. M.; Hwang, S. J.; Vincent, D.; Minnen, D.; Baluja, S.; Covell, M.; and Sukthankar, R. 2016. Variable Rate Image Compression with Recurrent Neural Networks. In *International Conference on Learning Representations*.
- Toderici, G.; Timofte, R.; Ballé, J.; Agustsson, E.; Johnston, N.; and Mentzer, F. 2020. Workshop and Challenge on Learned Image Compression (CLIC). <http://www.compression.cc>.
- Toderici, G.; Vincent, D.; Johnston, N.; Jin Hwang, S.; Minnen, D.; Shor, J.; and Covell, M. 2017. Full Resolution Image Compression With Recurrent Neural Networks. In *Proceedings of the IEEE Conference on Computer Vision and Pattern Recognition (CVPR)*.
- Vaswani, A.; Shazeer, N.; Parmar, N.; Uszkoreit, J.; Jones, L.; Gomez, A. N.; Kaiser, Ł.; and Polosukhin, I. 2017. Attention is all you need. *Advances in neural information processing systems*, 30: 5998–6008.
- Wang, Z.; Simoncelli, E. P.; and Bovik, A. C. 2003. Multi-scale structural similarity for image quality assessment. In

The Thrity-Seventh Asilomar Conference on Signals, Systems & Computers, 2003, volume 2, 1398–1402. Ieee.

Wu, Y.; Li, X.; Zhang, Z.; Jin, X.; and Chen, Z. 2021. Learned block-based hybrid image compression. *IEEE Transactions on Circuits and Systems for Video Technology*.

Xie, Y.; Cheng, K. L.; and Chen, Q. 2021. Enhanced Invertible Encoding for Learned Image Compression. In *Proceedings of the ACM International Conference on Multimedia*.

Zhou, J.; Wen, S.; Nakagawa, A.; Kazui, K.; and Tan, Z. 2019. Multi-scale and context-adaptive entropy model for image compression. In *Proceedings of the IEEE Conference on Computer Vision and Pattern Recognition Workshops*.

Zhu, X.; Song, J.; Gao, L.; Zheng, F.; and Shen, H. T. 2022. Unified Multivariate Gaussian Mixture for Efficient Neural Image Compression. In *Proceedings of the IEEE/CVF Conference on Computer Vision and Pattern Recognition (CVPR)*, 17612–17621.

Zhu, Y.; Yang, Y.; and Cohen, T. 2022. Transformer-based Transform Coding. In *International Conference on Learning Representations*.

Zou, R.; Song, C.; and Zhang, Z. 2022. The Devil Is in the Details: Window-Based Attention for Image Compression. In *Proceedings of the IEEE/CVF Conference on Computer Vision and Pattern Recognition (CVPR)*, 17492–17501.